Potential of helicopter-based SkyTEM technology for imaging large landslides: Case study of Te Puia and Mangahauini landslides, Tairāwhiti Gisborne

RL Kellett
ST McColl
BJ Rosser

GNS Science Report 2025/04
December 2025

Earth Sciences
New Zealand

DISCLAIMER

BIBLIOGRAPHIC REFERENCE

Kellett RL, Rosser BJ, McColl ST. 2025. Potential of helicopter-based SkyTEM technology for imaging large landslides: case study of Te Puia and Mangahauini landslides, Tairāwhiti Gisborne Lower Hutt (NZ): Earth Sciences New Zealand. 42 p. (GNS Science report; 2025/04). https://doi.org/10.21420/XVJM-0Q68

RL Kellett, Earth Sciences New Zealand, PO Box 30368, Lower Hutt 5040, New Zealand
BJ Rosser, Earth Sciences New Zealand, PO Box 30368, Lower Hutt 5040, New Zealand
ST McColl, Earth Sciences New Zealand, PO Box 30368, Lower Hutt 5040, New Zealand

ISSN 2350-3424 (online)
ISBN 978-1-99-105889-8 (online)

CONTENTS

FIGURES

TABLES

APPENDICES

APPENDIX FIGURES

ABSTRACT

The Te Puia Springs and Mangahauini Gorge landslides are large features in the landscape of Tairāwhiti Gisborne. The movement of these landslides is recognised as a risk to the main highway around the East Cape (State Highway 35) and, in the case of Te Puia Springs, a direct risk to buildings and people in the village, which includes a regional hospital. The movement of Te Puia Landslide has been monitored for many decades. Landslides in Mangahauini Gorge have blocked the river and caused damage to the road on several occasions. The most recent movements during Cyclone Gabrielle in 2023 resulted in complete closure of the road through the gorge, and remedial engineering work is ongoing at a cost of millions of dollars.

The landslides are large and complex, so re-aligning the highway to avoid unstable ground is not practical. An airborne electromagnetic (AEM) survey was undertaken to research the utility of this method for investigating large complex landslides and placing the landslides in a regional context. The technology has been used elsewhere in New Zealand to map aquifers in the top 10–200 m and identify depth to bedrock in alluvial basins. In the investigation of landslides, geophysical data can provide some information on the physical properties of the material in the landslide, as well as the geometry of the landslide, provided that there is a contrast in properties with the underlying bedrock. The rock property derived from the AEM survey is electrical resistivity. Geologic materials demonstrate electrical-resistivity variations in relation to changes primarily in mineral composition, porosity, permeability and fluid saturation.

Seven lines of AEM data were collected over Te Puia Springs, and five lines were collected over the Mangahauini Gorge. The resulting resistivity models identified the deeper (50–250 m) bedrock geology, including layering in the Cretaceous and Cenozoic sediments of the East Coast Allochthon. The morphology of the bedrock units may have some influence on the geometry of the landslides but, to a first order, Te Puia Landslide is occurring within the thin Quaternary cover and/or weathered near-surface bedrock, mostly within the top 50 m. In some places, this layer is less than 10 m thick and the AEM method cannot image changes with any confidence. In contrast, Mangahauini Landslide has a deep-seated detachment surface (up to 150 m deep), and the block of high-resistivity sandstone in the main landslide may have undergone significant rotation. Slumping of the over-steepened toe of the rotated block produces secondary landslides into Mangahauini River.

The resistivity variations within both landslides are significant, so resolution of the mapping in future surveys could be increased by using closer-spaced lines and being closer to the ground. A different airborne system would be needed for this approach. Deploying ground-based systems in some of the terrain is also an option.

While it was not a primary objective of this work, the highly saline thermal waters at Te Puia Springs were imaged to depths of 150 m. There appears to be some influence of faulting and sedimentary layering on the distribution of low-resistivity zones associated with the saline fluids. The lines that crossed the prominent sinter at the surface showed that it was highly resistive and mappable. The results of this work provide motivation for considering AEM as a technique for mapping low-temperature geothermal systems.

KEYWORDS

Landslides, East Cape, Te Puia Springs, Mangahauini Gorge, airborne electromagnetic, geophysics, low-temperature geothermal

This page left intentionally blank.

1.0 Introduction

Landslides pose a substantial risk in New Zealand, with over 1500 deaths recorded since 1760 (Bruce 2022) and damages reaching billions (McMillan et al. 2023). Roading, pipelines, transmission networks and other infrastructure corridors are commonly affected by landslides and pose a major challenge for maintaining existing – and planning new – transport routes and infrastructure. For example, a 2011 rupture of the Maui gas pipeline in Taranaki due to landslide displacement is estimated to have a gross cost of $200 million (MBIE 2012). The cost to re-instate the coastal highway and railway corridor following landslide damage triggered by the 2016 Kaikōura earthquake was approximately $1.2 billion (Saul and Anderson 2019). In 2023, Cyclone Gabrielle caused severe disruptions to critical infrastructure networks across the North Island, particularly the transport network, requiring debris removal, repair or reconstruction and stabilisation of slope segments (Hastings District Council 2024). Across Hawke's Bay and Tairāwhiti Gisborne, Lin et al. (2025) identified nearly 700 landslides that either blocked or damaged a road during Cyclone Gabrielle, and Hastings District Council estimates $800 million and 7–10 years to repair and re-build the roading in their district (from both flood and landslide damage). Reducing landslide risk therefore has great economic and social benefit.

Better identification, measurement and understanding of the hazard can contribute to risk reduction. Identifying incipient landslides prior to their failure provides opportunity to avoid these, for example, during road-alignment investigations or when planning new housing developments. Measuring the depth (i.e. size) of landslides helps to quantify their potential hazard and may lead to mitigating the effects of landslide movement. Measuring the landslide geometry (e.g. failure-surface shape) and relationships to geological structures and groundwater helps to understand the causes of the landslide and anticipate its behaviour under changed conditions. Collectively, this information can be used to help mitigate landslides and reduce the risks these pose; however, it is often difficult and costly to collect.

Geophysical tools can be used to help identify, measure and understand landslides in non-invasive and cost-effective ways. Moreover, airborne geophysical methods offer the potential to survey large areas and avoid or lessen time-consuming ground-based methods that sometimes pose challenging access and safety issues for equipment and personnel. Airborne electromagnetic technology for subsurface surveying has been used in New Zealand for several years to successfully map groundwater reservoirs (Rawlinson et al. 2021). Outside of New Zealand, the technology has been applied to other applications, including landslide-risk investigation (e.g. Isacsson et al. 2021), but, to our knowledge, it had not been attempted in New Zealand. Ground-based electrical geophysical surveys have been applied to landslides within New Zealand with success (e.g. Singeisen et al. 2022), suggesting potential application of airborne approaches as well.

Here, we explore the potential of airborne electromagnetic technology for defining the boundaries, depth and geological context of large (10+ ha) landslides in a New Zealand setting. The study used the opportunity provided by a planned airborne electromagnetic (SkyTEM) groundwater survey in Tairāwhiti Gisborne Region to add a small amount of additional surveying of two landslides, which are hazards for local communities and infrastructure. We evaluate the use of the technology for application to landslide investigation and identify recommendations for improving the survey configuration and planning in the future.

2.0 Case-Study Landslides and Geological Context

The two landslide case studies are located within the East Cape, North Island, forming part of the accretionary prism of deformed marine sediments associated with subduction of the Pacific plate along the Hikurangi subduction margin. The stratigraphy includes Cenozoic marine sedimentary deposits, including crushed and deformed rocks of the East Coast Allochthon unconformably overlying Cretaceous meta-sedimentary basement rocks. Uplift, incision by rivers, weak rocks, recent deforestation and the incidence of earthquakes and heavy rainfall have made large, deep-seated rockslides and earthflows common in the hill-country terrain of the East Cape (Page et al. 2000). The two landslides are located at Te Puia Springs and along the Mangahauini Gorge upstream of Tokomaru Bay township (Figure 2.1).

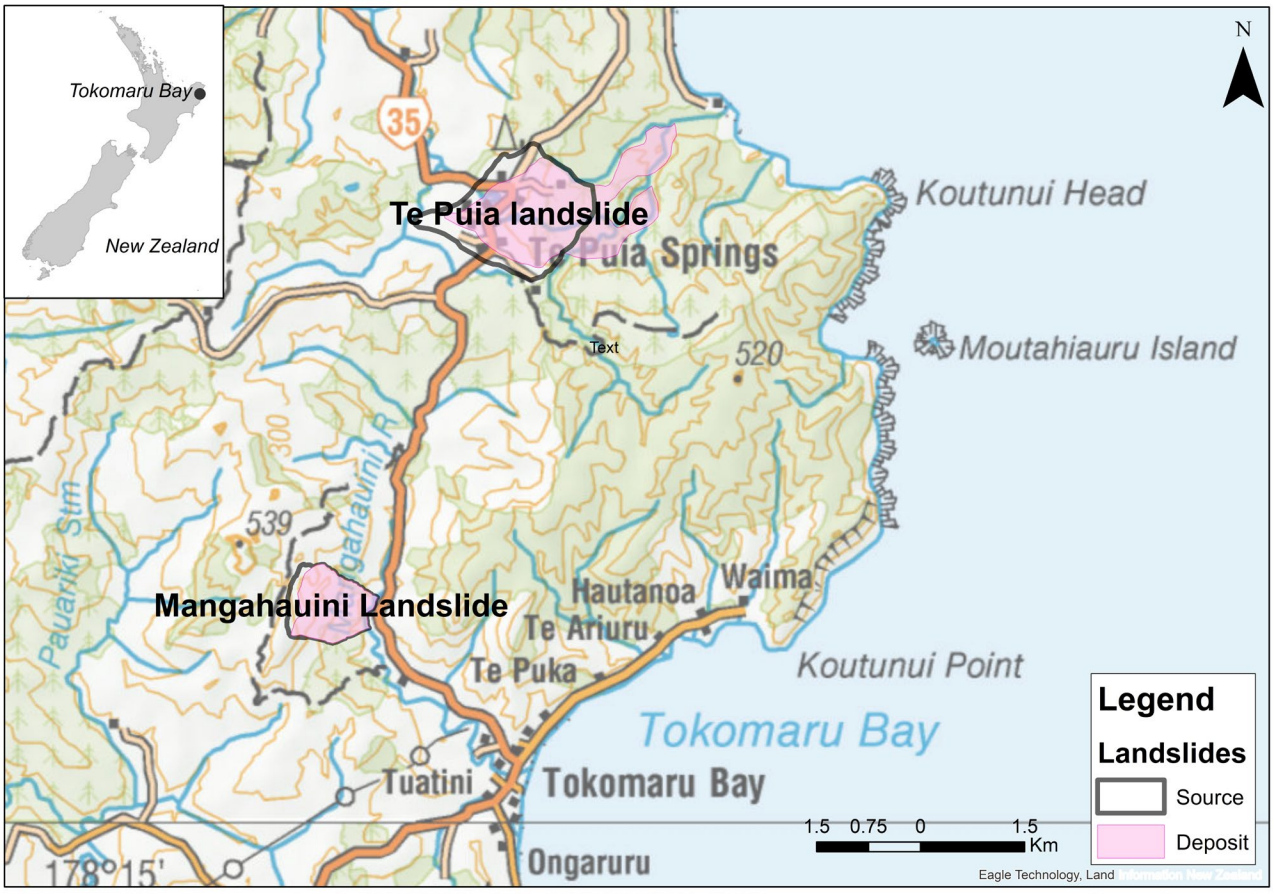

Figure 2.1 Location of Te Puia and Mangahauini landslides along State Highway 35, north of Tokomaru Bay, Tairāwhiti Gisborne. The boundaries of the source and deposit are outlined.

2.1 Te Puia Landslide

Te Puia Landslide is an approximately 300 ha active, deep-seated, slowly creeping landslide (Figure 2.2). At Te Puia, Cretaceous units of the East Coast Allochthon overlay and are surrounded by Neogene sediments. A large (700–20 m wide) calcareous sinter deposit is present, along with several active thermal springs, pools and gas vents (Pohatu et al. 2010). Mazengarb and Speden (2000) suggest that the east–west orientation of the sinter deposit may be related to a fissure associated with the active Te Puia Landslide, which in turn may have been influenced by alteration and wetting by geothermal water.

According to Mazengarb and Speden (2000), the landslide deposit consists mainly of large sliding blocks (likely geothermally altered) of Late Cretaceous bedrock transitioning to an earthflow at the landslide toe. Surveying by the Department of Lands and Survey in the 1970s, reported by Gibb (1981) suggested a movement rate of about 5 cm per year in the main body, with likely faster movement in the earthflow. Surveys by the Engineering Geology Section of the New Zealand Geological Survey described the geometry of the landslide and possible mechanism of formation, as well as recommended drilling and hydrogeological studies (Oborn 1980).

State Highway 35 crosses the landslide, and the Te Puia Springs settlement is located on the landslide. Damage from gradual movement has been reported (Impact Consulting Ltd 2018), providing motivation for understanding more about the geometry, volume and relationship to the geology through selecting this landslide as a case study for the SkyTEM surveys.

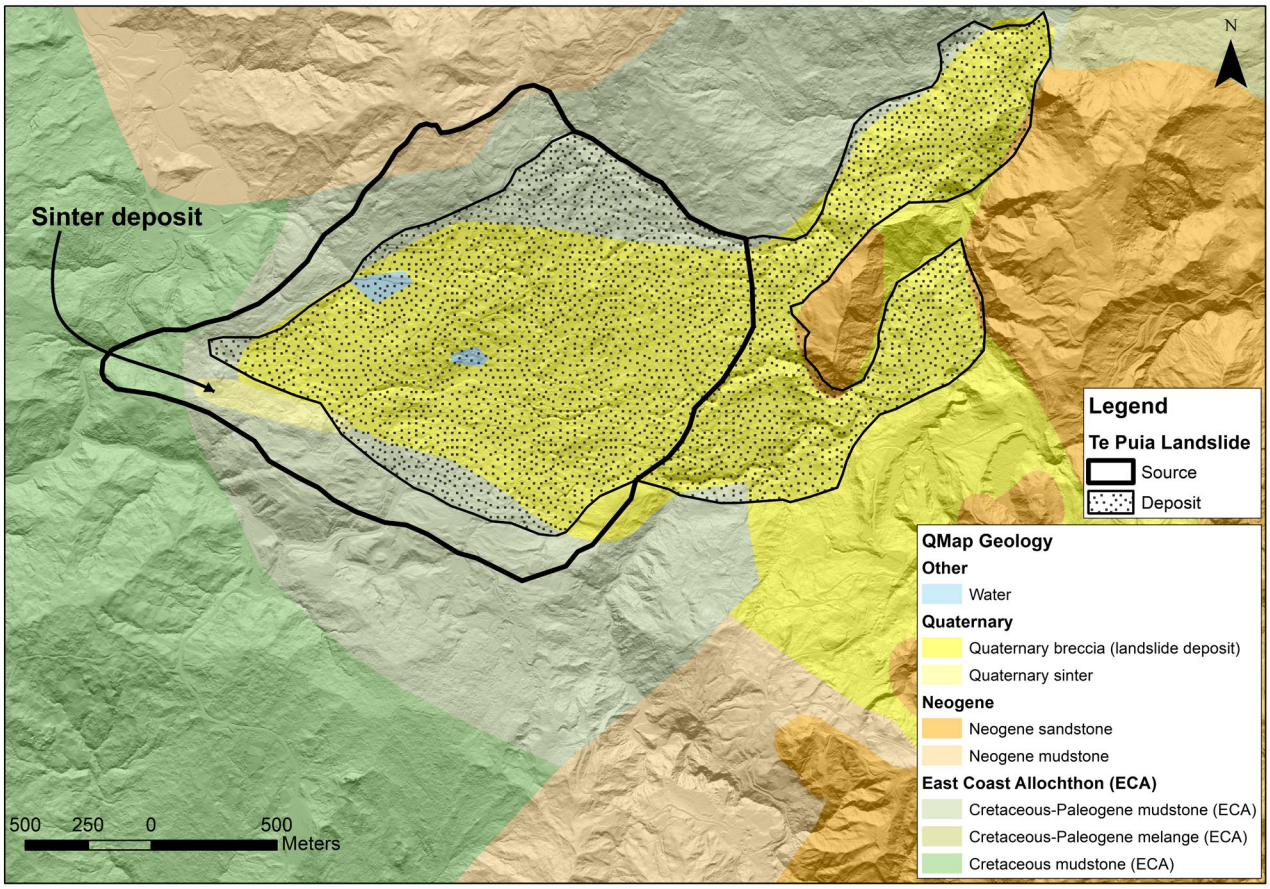

Figure 2.2 Geology of the Te Puia area (simplified from Mazengarb and Speden [2000]) with the inferred boundary of the Te Puia Landslide source area and deposit.

2.2 Mangahauini Landslide

'Mangahauini Landslide' is the name given to one of several large, deep-seated landslides identified along the Mangahauini River corridor, upstream of Tokomaru Bay township (Figure 2.3). The large landslides in this area are predominantly formed within Neogene mudstones and are commonly found where river incision has produced steep slopes. Little is known of the activity and movement rates of the landslides, but these are assumed to be slow moving or have potential to re-activate. Re-activation may involve the entire landslide, or smaller secondary (i.e. parasitic) failures of the main bodies, for which there is geomorphic and historical evidence (Figure 2.3). A relatively shallow ~20 ha part of the ~100 ha deep-seated Mangahauini Landslide failed rapidly during Cyclone Gabrielle in February 2023, forming a temporary blockage of Mangahauini River (Wolter et al. 2023). Lakes that impound behind landslide dams pose a threat to infrastructure and communities upstream, and rapid breaching

of the dam can cause high-discharge floods that can impact downstream infrastructure and communities. While the 2023 landslide blockage did not result in a damaging flood, based on the presence of several large landslides and previous landslide dams, there is clearly potential for large landslide dams to form in the future. This risk has provided motivation for selecting Mangahauini Landslide for the second SkyTEM case study.

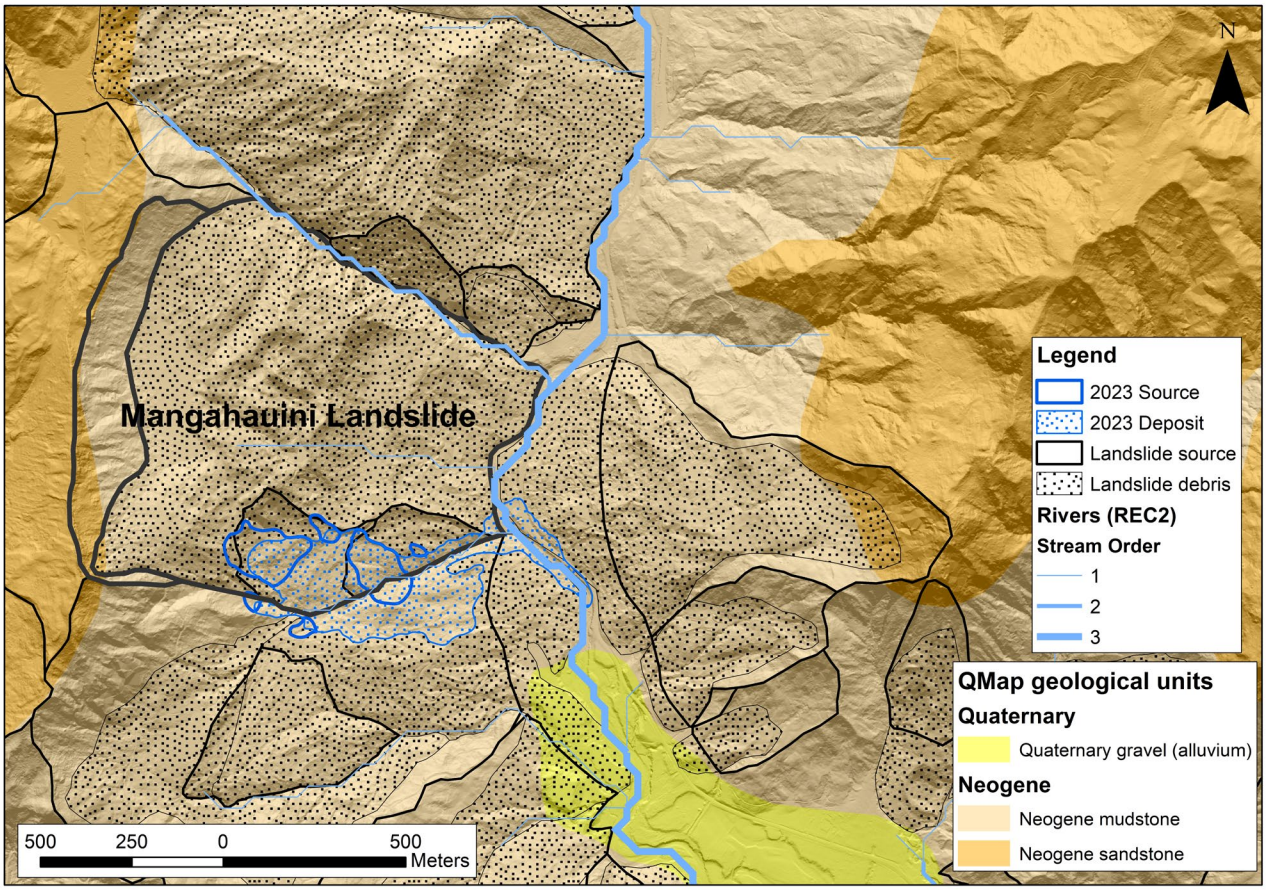

Figure 2.3 Geology of the Mangahauini Landslide area (simplified from Mazengarb and Speden [2000]), showing source areas and deposits of large landslides mapped in the area. Mangahauini Landslide is approximately in the centre of the map, with blue stippled polygons showing the 2023 parasitic failure that produced a temporary landslide dam during Cyclone Gabrielle.

2.3 Stratigraphy

The stratigraphy used in the interpretation of the SkyTEM data presented in this report is summarised from the QMAP 1:250,000 map sheet (Mazengarb and Speden 2000) and adapted for the geological maps shown in Figures 2.2, 2.3 and 2.5. Figure 2.4 shows the key stratigraphic units in the study area (including in nearby borehole logs) relevant to the depth of investigation of the SkyTEM system; not all of these units are shown in the geological maps presented in this report.

Age	Unit	Group	Qmap	Formation	Dominant Lithology
Quaternary			Q1l	Landslide deposits	Breccia
			Q1	Sinter deposits	Sinter
			Q1	Alluvial deposits	Gravel
Neogene		Mangaheia Gp	Mmk	Tokomaru	Sandstone
Neogene		Tolaga Gp	Mlr	Areoma Fmn	Sandstone
			Ml	Undifferentiated	Mudstone
Paleogene Cretaceous		Tinui Gp	Kiw	Whangai	Mudstone
Cretaceous		Ruatoria Gp	Kri	Tikihore Fmn	Mudstone
			Krm	Mokoiwi Fmn	Mudstone
			Krt	Taitai Fmn	Sandstone

Figure 2.4 Stratigraphy in the SkyTEM survey region. Mangaheia, Tolaga, Tinui and Ruatoria groups (Gp) are the main divisions in the stratigraphy. The formations of the units in the study area are listed along with the dominant lithology. The assigned colours match Figures 2.2, 2.3 and 2.5 where some units are not differentiated for simplicity. Not all of these units appear in the geological maps presented in this report.

The geological setting of this portion of the Raukamara Peninsula is complicated by the presence of the East Coast Allochthon. The geological framework for interpreting the region has changed over the last 50 years. Where possible, the current interpretation updates some older sections using the more recent description of the geological units (Mazengarb and Speden 2000). The geological units exposed at the surface in the Te Puia and Mangahauini area include Late Cretaceous Ruatoria Group; Paleogene Tinui Group mudstones; Neogene sandstones, siltstones and mudstones of the Tolaga Group; Neogene sandstones of the Mangaheia Group; and Quaternary alluvial deposits (Figure 2.4).

Many of these units are brecciated and included in the East Coast Allochthon as blocks or a melange. The blocks are bounded by thrust faults, and the strata have a regional dip of 20–30° to the north and northeast. The late Cretaceous and Paleogene units form large sheets that are thrust over complexly folded units in the underlying autochthonous basins. The emplacement of the East Coast Allochthon occurred in the early Miocene, further complicating the Neogene deposits (Mazengarb and Speden 2000) and resulting in highly crushed and sheared rock units that are very susceptible to erosion (Marden et al. 2008). In places, Neogene sedimentary basins were carried as piggy-back basins within the allochthon during the allochthon emplacement thrusting.

The Quaternary alluvial deposits lie in the valley floors. In the vicinity of Te Puia Springs, the Quaternary and Holocene units also include the sinter that forms a prominent topographical ridge along the line of the modern springs, as described in Section 2.1 (Glover 1968; Pohatu et al. 2010).

The landslide material at Te Puia includes Quaternary alluvial deposits and sinter, as well as blocks of Paleogene and Cretaceous rock. The landslide source region is located on top of Cretaceous mudstone to the west and Neogene siltstone and sandstone to the east.

In Mangahauini, the landslide source region is primarily in the Neogene mudstone and sandstone. The deposit overlays both Neogene mudstones in the gorge and Quaternary alluvial sediments in the river valley.

2.4 Boreholes

There are very few boreholes in the vicinity of the two airborne surveys (Figure 2.5). The petroleum well Te Puia-1 is located 5 km to the northwest of Te Puia Landslide (Laing 1972) on the northern edge of a block of allochthonous Cretaceous units. The well was drilled to a depth of 2040 m. The top 360 m of the well are summarised in Figure 2.6. The upper section of the well encountered 165 m of Cretaceous siltstone and sandstone, described by Laing (1972) as Taitai Sandstone. This unit corresponds to the Ruatoria Group unit that occurs on topographic high points (Taitai Sst : Krt; Mazengarb and Speden 2000).

The geophysical logs collected through the upper section of the well (gamma log) show alternating layers of silty and sandy material with typical bed thicknesses of 8–10 m. From 0 to 80 m depth, the unit is dominated by siltstones, with some prominent sandstone beds indicated in cuttings and the gamma signature. From 80 to 170 m depth (metres below ground level), the formation is characterised by massive siltstone beds, and the gamma-ray signature increases, showing a higher clay content. Between 170 and 175 m depth, the gamma signature increases to indicate a mudstone. The surface-casing was set at 175 m depth at the base of the Taitai Sandstone, so some of the character is due to the casing changes.

From 175 to 267 m depth, the lithology is described as undifferentiated siltstone, mudstone and sandstone pebbles associated with the Mokoiwi Breccia (Laing 1972). This unit is re-interpreted today as the Cretaceous Mokoiwi Formation in the Ruatoria Group (Figure 2.4; Krm; Mazengarb and Speden 2000). The bedding is 4–5 m thick and alternates from siltstone to mudstone. The induction resistivity log shows that the silty units have a resistivity of up to 15 ohm-m, while the mudstone units are 4–5 ohm-m.

Based on the mapping of Mazengarb and Speden (2000), the geological units between the Te Puia-1 well and Te Puia Landslide are interpreted to be in the Cretaceous Ruatoria Group, primarily Mokoiwi Formation with isolated areas of Taitai Sandstone on topographic high-points (Figure 2.5). The geological layering and resistivity properties described in Te Puia-1 are used to support the interpretation of the deeper parts of the SkyTEM sections at Te Puia in Section 5.3.

The shallow borehole GGR008 was drilled in 1994 at the Te Puia transfer station. It extends to 1.8 m depth and encountered topsoil, gravel and clay. Similarly, the two bores located in Tokomaru Bay were drilled to 1.5 m depth and encountered silt and pebbles. Recent drilling has been undertaken in the Mangahauini Gorge, but the results are not available for this interpretation.

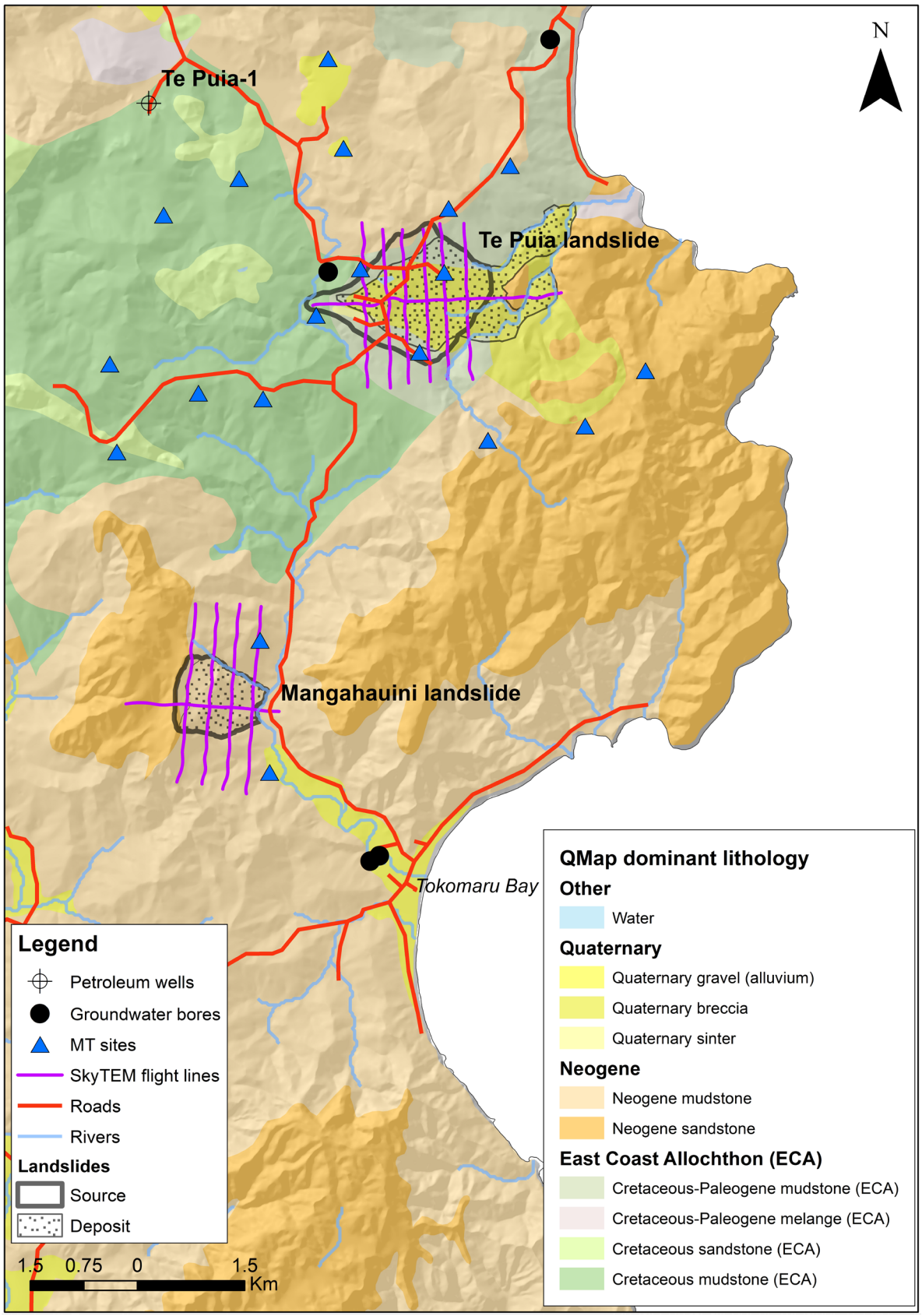

Figure 2.5 Location of previous geophysical and ground investigations in the Te Puia and Mangahauini areas, along with the mapped landslides and SkyTEM survey lines. Te Puia-1 is a petroleum exploration well, and the other boreholes are shallow groundwater or geotechnical engineering test holes. The positions of several magnetotelluric (MT) stations are also shown. The geology data are simplified from Mazengarb and Speden (2000), and other landslides in the region (other than Mangahauni and Te Puia) have been excluded for visual simplicity.

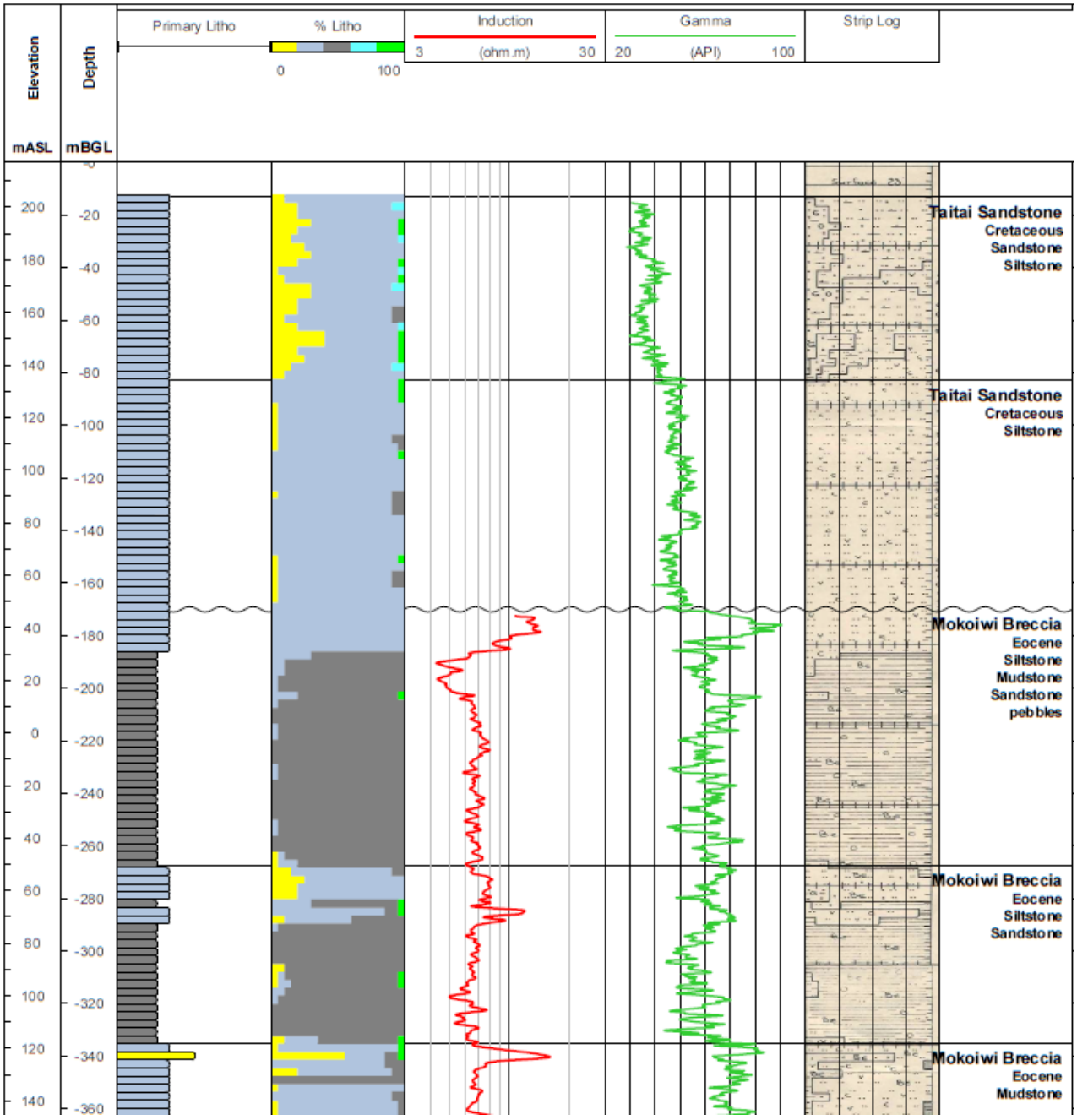

Figure 2.6 Composite log from the Te Puia-1 petroleum well. The top 360 m have been re-produced from the original petroleum report (Laing 1972). The tracks presented are: (1) primary lithology; (2) percentage clay (dark grey), silt (grey), sand (yellow), carbonaceous (green) and shelly material (cyan); (3) induction resistivity log; (4) natural gamma log; (5) original composite log; and (6) original formation description.

2.5 Geophysical Surveys

Petroleum exploration undertaken between 1960 and 2000 included seismic surveys in the area west and south of Tokomaru Bay, but no detailed work was done through the Mangahauini and Te Puia area. The most comprehensive geophysical work undertaken at Te Puia and Mangahauini was part of an investigation of low-temperature geothermal resources (Zygadlo et al. 2015). A combination of broad-band magnetotelluric (MT) stations supplemented by high-frequency audiomagnetotelluric measurements (AMT) was used to image the subsurface from 100 to 10,000 m depth (see Figure 2.5 for locations of the sites). The survey included data from the regional survey of the Raukumara Peninsula (Heise et al. 2013). The key output of the detailed survey is a cross-section through Te Puia Springs showing the general pattern of low-resistivity sedimentary units extending to 2 km depth over a high-resistivity greywacke basement. More detail in the vicinity of the springs includes some differentiation of the faults that separate different blocks. In general, the resistivity contrasts in the sedimentary section are subtle (1–3 ohm-m), and the authors concluded that it would be challenging to separate different sedimentary units or identify the geothermal fluids based on resistivity. The report commented on the likelihood of the sinter at Te Puia being highly resistive, but it was not resolved by the AMT/MT survey. The entire landslide area was described as Q1 deposits and interpreted to be in the order of 200 m thick, but the resistivity was similar to the underlying Neogene sediment.

3.0 SkyTEM Technology

SkyTEM is a specific airborne geophysical technique that uses transient (time-domain) electromagnetics (TEM) to investigate the shallow (up to ~500 m deep) electrical-resistivity structure of the Earth (Sørensen and Auken 2004). The resistivity structure can then be interpreted in terms of subsurface geology and used to inform and improve existing geological models. Data are collected using specialist equipment slung beneath a helicopter and flown at low elevations along closely spaced lines. A key advantage of this technique is that it enables a large amount of high-resolution data to be collected quickly and cost-effectively.

Figure 3.1 shows the SkyTEM system with the hexagonal frame slung beneath the helicopter. The lengths of the frame sides are approximately 12 m. The transmitter loop is extended around the entire loop. There are two separate transmitter loops. The low-moment (LM) transmitter is a single strand of wire that provides a very rapid turn-off and is sensitive to the shallow geology. The high-moment (HM) transmitter has six loops of wire and can transmit a larger current to enable deeper penetration of the signal.

The receiver coils are mounted in the tail section of the frame. One feature of the SkyTEM system is the position of the receivers close to the zero-coupling point with respect to the primary magnetic field, increasing the sensitivity of the instrument. There are two receiver coils, referred to as the 'Z coil' and 'X coil'. The Z coil is placed approximately 2 m above the frame and provides the data most commonly used in data processing. The X coil provides a measure of lateral continuity of the geology and is used in regions with steeply dipping geological units, such as those commonly encountered in mineral-exploration projects.

The instruments needed to determine the position of the system (GPS, laser altimeters and tiltmeters) are located near the front of the loop. A magnetometer is positioned on a probe ahead of the loop to provide measurements of ambient magnetic field. The transmitter controller is slung above the loop, and the generator used to power the loop is suspended closer to the helicopter to reduce electrical interference with the system. A downward-facing camera is mounted on the helicopter to provide an additional check on the attitude of the loop and its location relative to features on the ground.

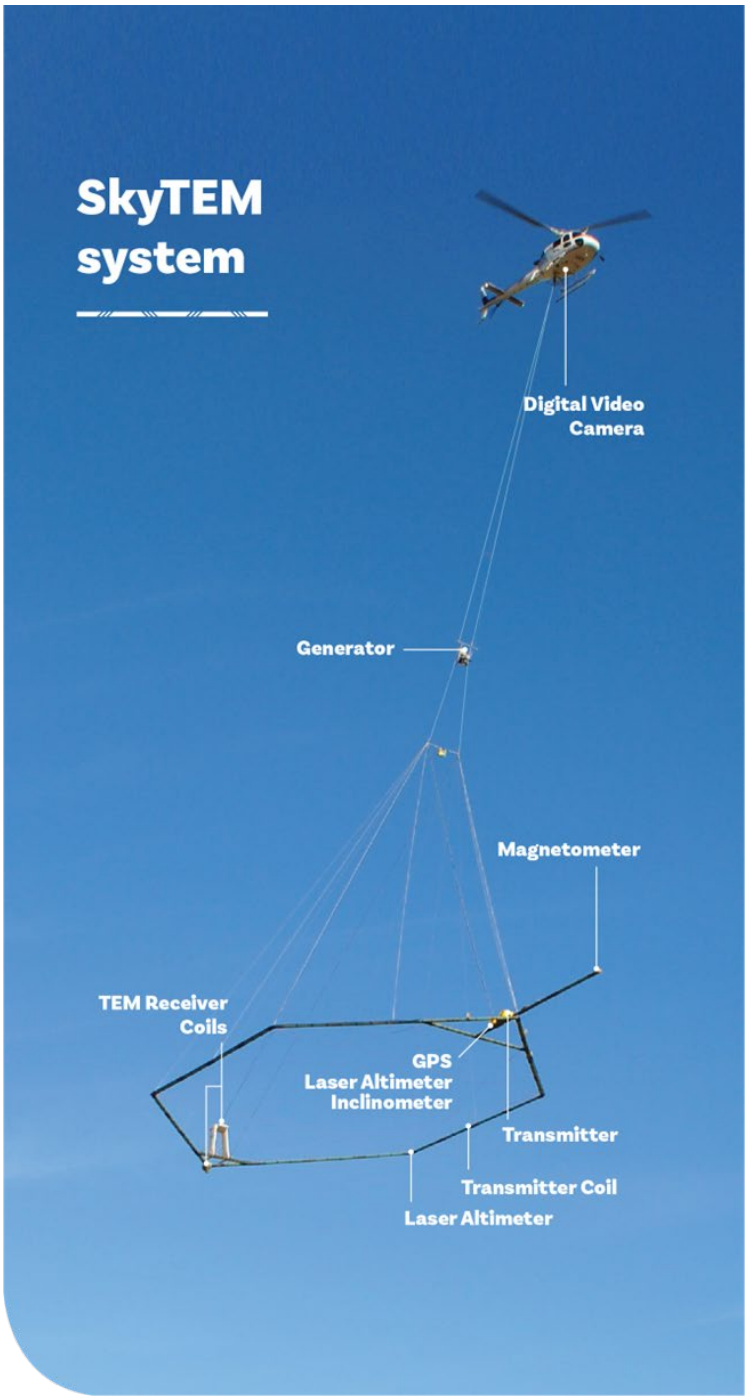

Figure 3.1 The SkyTEM system. The transmitter frame holds the transmitter loop, inclinometers, laser-altimeters, receiver coils and instrumentation (Sorensen and Auken 2004). Figure from SkyTEM Australia Pty Ltd.

The system deployed for this project is the SkyTEM 306HPM. The details of the system are given in Tables 3.1 and 3.2. The transient electromagnetic system is characterised by the waveform of the transmitter current (Figure 3.2). The LM waveform has a short 'on' time, with a rapid increase in current, and a sharp 'turn-off' time that enables shallow signals to be detected. The HM waveform transmits the current for longer, producing a deeper penetration of the signal, and the current turn-off time is longer, making it less sensitive to the shallow structure. The SkyTEM system switched back and forth between the HM and LM signal at a frequency of 25 Hz. The data are collected automatically for the entire flight of the helicopter, enabling the pilot to focus on following the flight plan. The received data are recorded digitally and can be stacked to reduce noise once the survey flight has been completed. The number of stacks is determined by the speed of the helicopter and noise in the data.

Table 3.1 Summary of low-moment and high-moment transmitter (Tx) and receiver (Rx) specifications.

Parameter	Low Moment	High Moment
Number of turns	1	6
Transmitter area	342 m^2	342 m^2
Tx current	8 A	220 A
Tx peak moment	~ 4000 Am^2	~ 450,000 Am^2
Repetition frequency	25 Hz	25 Hz
Tx-on-time	1000 µs	5000 µs
Tx-off-time	1018 µs	15000 µs
Duty cycle	66%	25%
Wave form	See Figure 3.2	See Figure 3.2

Table 3.2 Effective area of X and Z receiver coils.

Parameter	X	Z
Rx coil effective area	115 m^2	325 m^2
Rx coil low pass cut-off frequency	341.6 KHz	206.8 KHz

The receiver records the change in secondary electromagnetic field caused by the decay of the electric current in the ground following the shut-off of the transmitter. The data are recorded in windows through the off-time. The LM signal is sampled in 25 windows from 0 µs to 423 µs. The HM signal is sampled in 41 windows from 0 µs to 10,100 µs.

The flight altitude depends on the flight speed, topography and presence of obstacles such as towers, tall trees and buildings. Over forested areas, the altitude is increased to maintain safe clearance over the treetops. The nominal flight altitude for this survey was 51 m (frame height). The average terrain clearance was 70 ± 16 m.

The flight speed can be adjusted to balance survey time, data density on the ground, smearing of data recovered at depth and a more stable levelling of the transmitter loop. For this survey, flight speeds ranged between 64 and 118 km/hr, with a mean (± standard deviation) speed of 88 ± 9 km/hr.

For this survey, data were provided to GNS Science in April 2024 as averaged ('stacked') 5 Hz data and re-sampled to a XYZ ascii file with a running mean of 0.5 s (2 Hz). Given the flight speed, this means that the theoretical (5 Hz) average distance between sample points (in-line) is approximately 5 m, but the smoothing distance (set by the running mean) is 12 m.

The penetration depth for the SkyTEM system depends on the transmitter moment, receiver sensitivity, geological setting (bulk resistivity), background noise level, flight speed and altitude. Normally, a penetration depth of 150–500 m is expected for surveys using this equipment. During the inversion, an actual depth of investigation (DOI) is estimated for each set of measurements. In moderate resistivity terrains, such as the East Cape, the DOI is restricted to 200 m.

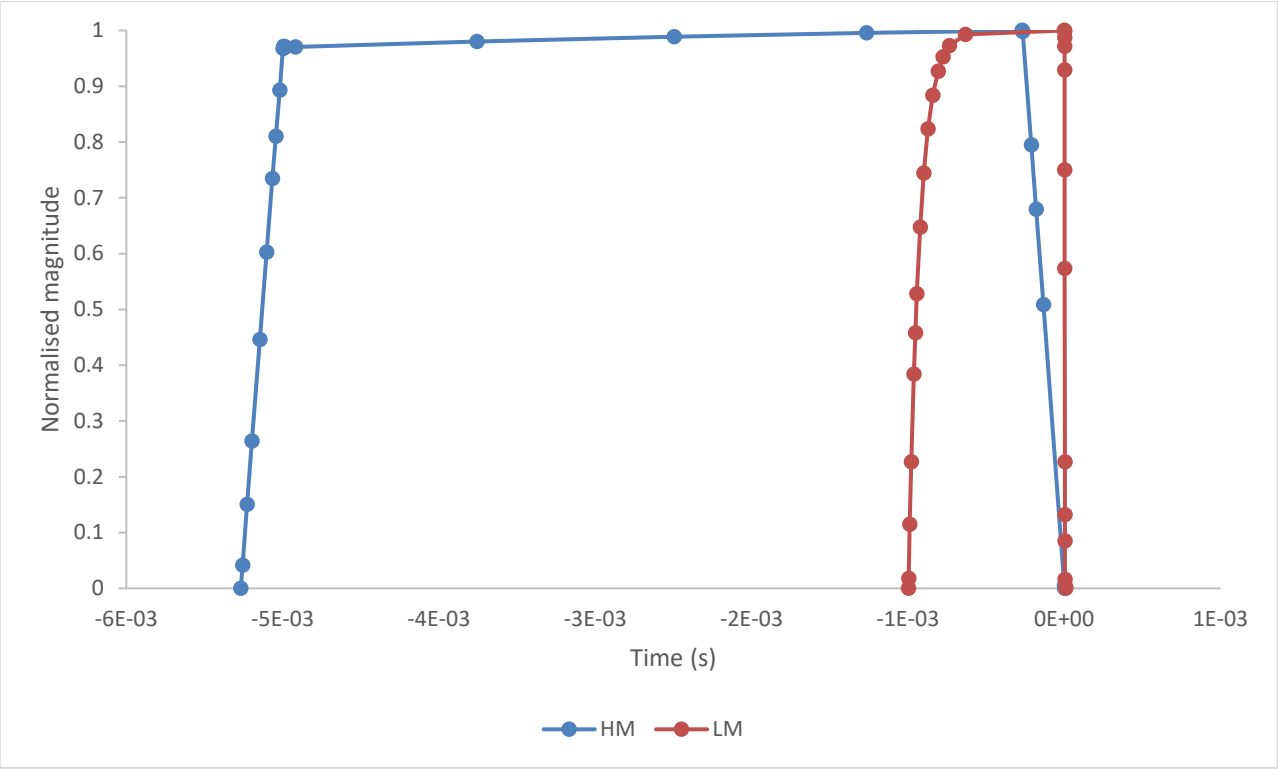

Figure 3.2 Waveform of the signal for the high-moment (HM) and low-moment (LM) cycles. The 'on' time for the current pulse indicates when the current ramps up to full current. The 'off' time starts at time zero on the figure, and the received signal is recorded during the 'off' time.

SkyTEM data are processed through to an electrical-resistivity model at each ground point covered by the surveying. The processing to produce the resistivity model is discussed in more detail in Section 4. Electrical resistivity is among the most widely used geophysical property in groundwater exploration, geotechnical and environmental investigations (Reynolds 2011). It is related to the ability of a volume of rock to transmit electric current. The International System of Units (SI) unit for resistivity is ohm-m, and the inverse is electrical conductivity (10 ohm-m = 0.1 S/m). In geotechnical investigations, resistivity is the preferred measurement and is the term adopted in this report. For reference, in groundwater and geothermal fluid studies, electrical conductivity is preferred and often expressed in mS/m or μS/cm (1 ohm-m = 1000 mS/m = 10,000 μS/cm).

Some geophysical methods rely on directly injecting electrical current into the ground to determine the resistivity. The SkyTEM method induces electric current to flow by electromagnetic induction, but the result is the same measurement of resistivity. For the SkyTEM system, the vertical resolution of the model is approximately 0.5 m near the surface and 10 m at the DOI (150–200 m).

4.0 Methodology

The survey was planned in consultation with geologists familiar with the structure of the landslides in area. The SkyTEM crew were transiting between a groundwater project in Tolaga Bay and Tairāwhiti Gisborne, so were able to complete two small surveys in the Te Puia and Mangahauini areas.

The aim of the survey was to test the resolution and application of the SkyTEM system in a landslide setting and to provide a general 3D view of the landslide features. Each grid comprised a series of flight lines approximately 2.2 km long and a perpendicular tie-line (3.4 km long at Te Puia and 2.1 km long at Mangahauini). A total of 28.67 line-km of survey were completed. Table 4.1 gives the locations of the end points of each line.

The flight lines were positioned to cross from country rock onto the landslide and to be approximately parallel to the direction of movement. However, for a three-dimensional feature such as a landslide with poorly defined boundaries, it is difficult to position the lines optimally. A major factor in designing the survey is the suitability of the terrain for helicopter flight, as well as the locations of roads, powerlines and buildings. Powerlines and buildings are sources of electrical noise and are best avoided. Roads and other linear corridors are best crossed at right angles to minimise the impact on the data.

Figure 4.1 shows the location of the survey lines on Te Puia Landslide, and Figure 4.2 shows the survey line grid over Mangahauini Landslide.

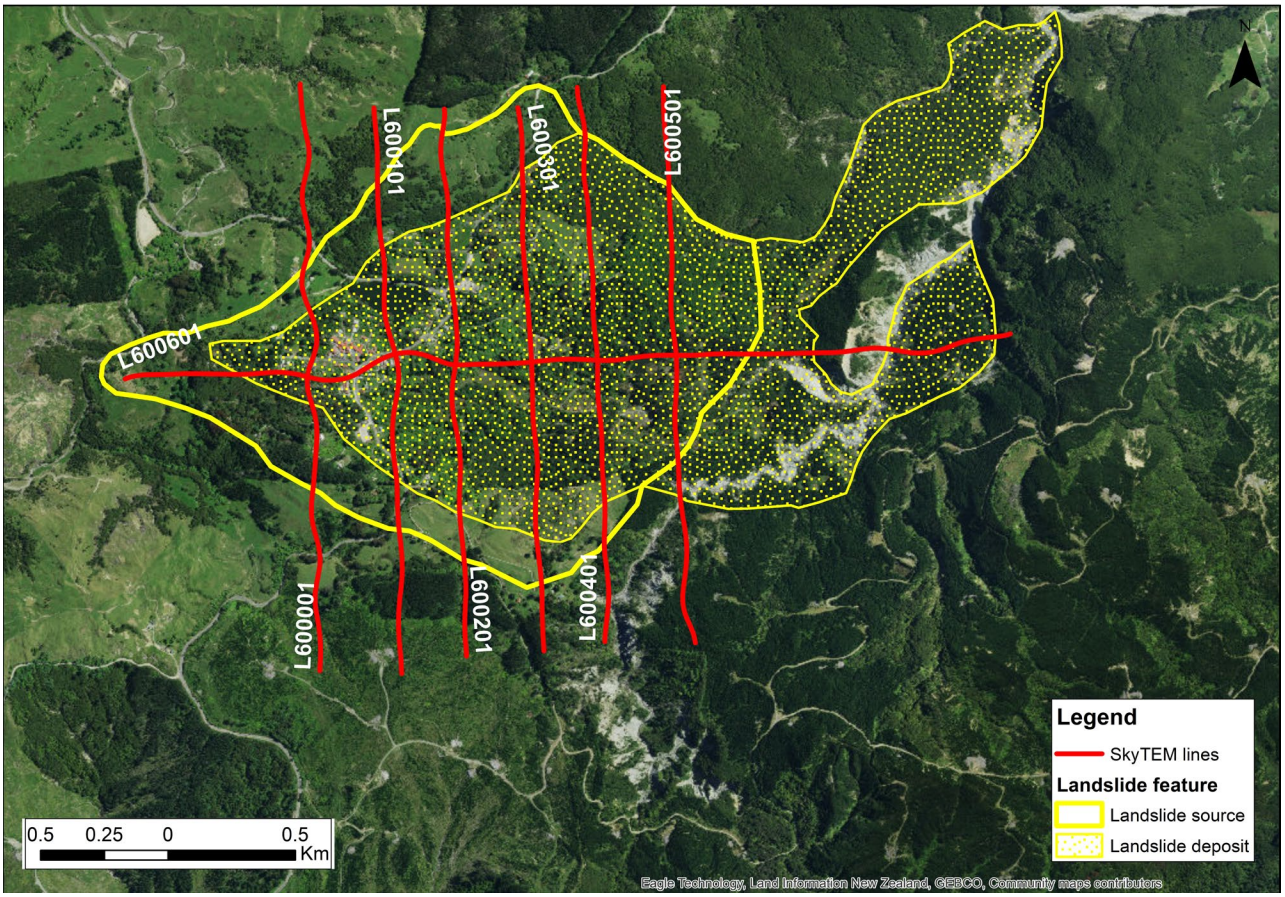

Figure 4.1 Location of the SkyTEM survey lines in the Te Puia Springs area.

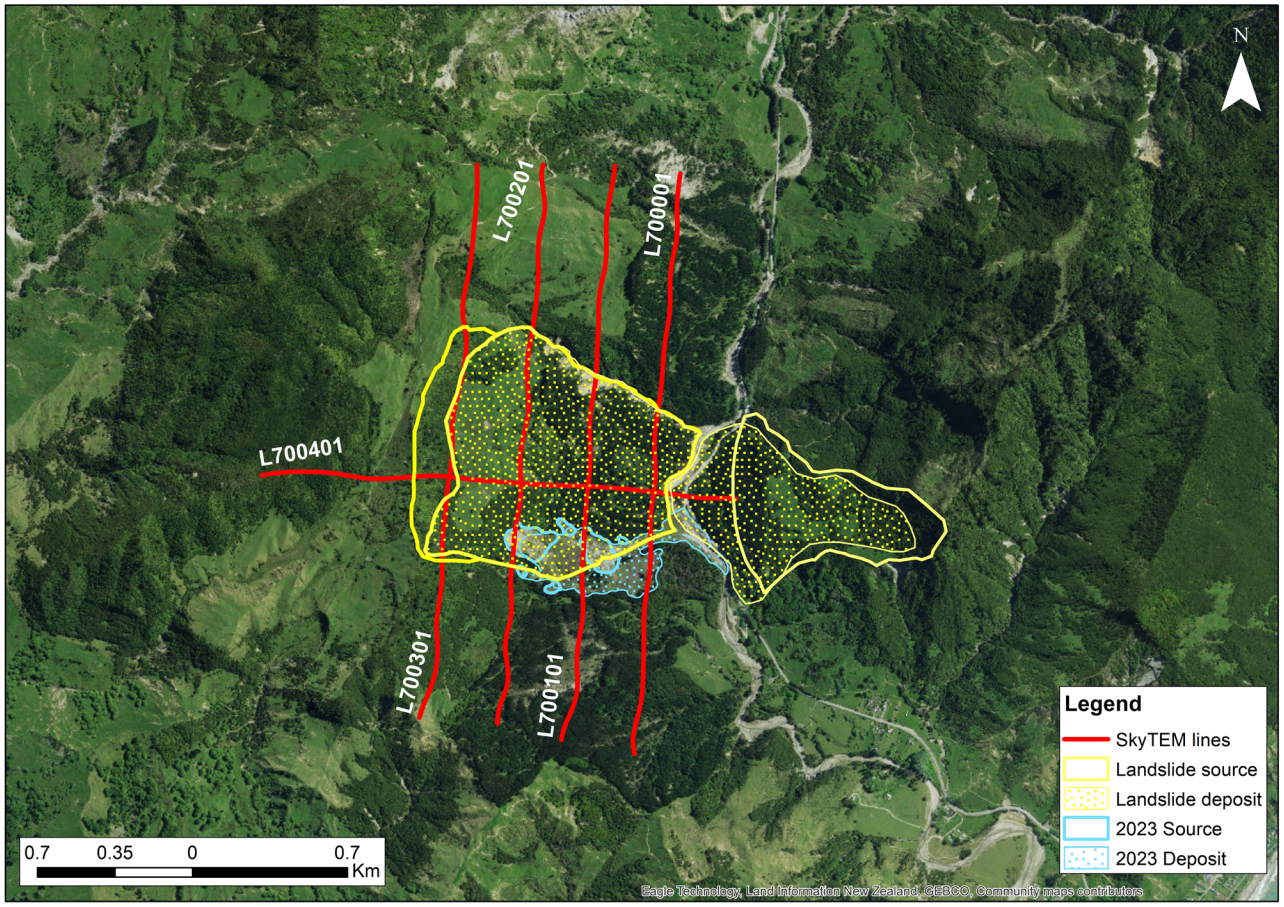

Figure 4.2 Location of the SkyTEM survey lines in the Mangahauini area. Here, the outlines of only Mangahauini Landslide (and the 2023 parasitic failure) and another large landslide on the opposing slope of the eastern side of the valley are depicted. For visual clarity, other landslides in the area are not shown.

Table 4.1 Summary of survey line locations.

Location	Line Number	East – Start	North –Start	East – End	North – End	Length (km)
Te Puia	L600001:21101	2065380	5775709	2065456	5773507	2.24
	L600101:21101	2065665	5775679	2065776	5773533	2.16
	L600201:21101	2065928	5775675	2066028	5773552	2.13
	L600301:21101	2066231	5775680	2066331	5773576	2.11
	L600401:21101	2066465	5775746	2066588	5773594	2.16
	L600501:21101	2066802	5775757	2066916	5773626	2.14
	L600601:21101	2064688	5774610	2068077	5774778	3.44
Mangahauini	L700001:21101	2063753	5767856	2063963	5770379	2.54
	L700101:21101	2063431	5767857	2063670	5770433	2.60
	L700201:21101	2063140	5767915	2063354	5770438	2.55
	L700301:21101	2062789	5767948	2063049	5770437	2.52
	L700401:21101	2062146	5769052	2064217	5768930	2.08

The survey was completed on 10 February 2024 and flying conditions were fair. A detailed report on this acquisition is included in the report for the larger groundwater project (SkyTEM Australia Pty Ltd 2024). The data were verified for quality and compliance to the planned flight lines as part of the survey management for the larger groundwater project. SkyTEM Australia processed the data in its Perth office using standard processing routines (SkyTEM Australia Pty Ltd 2024). A copy of the acquisition report and processed data was available within six weeks of the completion of flying on 18 February 2024.

The products delivered to GNS Science in April 2024 included:

- An acquisition report.
- Maps of the survey lines (*.pdf* and vectors in GIS-format files *.shp*).
- Maps of the elevation data (digital elevation model [DEM]), magnetic anomaly, powerline noise (*.pdf* and vectors in GIS-format files *.shp*).
- Maps of the electromagnetic amplitude for several gates (*.pdf* and vectors in GIS-format files *.shp*).
- Grids of the DEM, magnetic anomaly and all electromagnetic gates (Oasis Montaj *.grd*).
- Inversion models for each profile in *.png* and *.kmz* file formats.
- Grids of inversion models as an Oasis Montaj database (*.gdb*); ASCII XYZ format; Oasis Montaj *.map* and *.grd* format; *.pdf* and *.tiff* maps.
- Raw data in Oasis Montaj database (*.gdb*) and ASCII XYZ formats.

The processing included correction of the raw data for tilting of the loop during surveying; correction of the elevation data to remove incorrect altitudes due to steep terrain or tall trees; and removal of spurious data due to roads, powerlines or houses. A smoothing function was applied to the data depending on the individual time-gates to remove small variations caused by the motion of the helicopter (Auken et al. 2009). The magnetic field data were corrected for diurnal fluctuations of the Earth's field using a base station located close to the survey.

The processed data were then run through a smooth, spatially constrained inversion that derives a resistivity versus depth model for every measurement point along each flight line (Auken et al. 2015). The spacing of the models is approximately 5 m. The inversion model comprises 30 layers with electrical resistivity (ohm-m) varying smoothly from one layer to the next and from one sounding to the next. The shallowest layer was 4 m thick, and the deepest layer was 584 m below the ground surface. In line with common practise for geotechnical applications, we present the model as resistivity (instead of the reciprocal conductivity, S/m). Smooth inversions are biased against sharp boundaries, so, in some places, the depth to a major change in geology was not recovered in detail. Alternative approaches to detecting sharp boundaries can be employed, but, as a first approximation, the smooth inversion performs well for the shallow geology. The DOI is determined by the signal-to-noise ratio in the system and the bulk resistivity of the Earth materials. A DOI was calculated for each model and saved in the output to identify the depth below which the model has lower confidence.

Earth Sciences New Zealand has reviewed the inverted data in order to make some initial assessments of the results. The raw data were imported into a software package (Seequent AGS Workbench) and additional editing undertaken to reduce the noise and check for subtle effects of electromagnetic coupling between man-made objects and the SkyTEM system. A new inversion was undertaken on the edited data. The new inversion comprised a 40-layered model with a starting layer of 2 m thickness and a depth of 300 m to the basal layer. The aim of this model was to derive more detailed information about the subsurface geology.

The final models can be visualised in software such as Seequent AGS Workbench or LeapFrog. Additional information such as the geological map, boreholes and ground geophysical data can be used to help interpret the SkyTEM models.

5.0 Results

The results of the survey are shown for each area in the next sections. The models are represented as a cross-section in electrical resistivity (ohm-m) suspended under the topography defined by a DEM (LINZ 2021).

Geologic materials demonstrate electrical-resistivity variations in relation to changes primarily in mineral composition, porosity, permeability and fluid saturation (Palacky 1987). In geotechnical investigations of unconsolidated (typically Pleistocene to Holocene) sediments, the units with high resistivity (>200 ohm-m) are related to coarse-grained sand and gravel-rich layers, while units with low resistivity (<10 ohm-m) correspond to more fine-grained geologic materials such as silt and clay. In more consolidated rocks of deep-marine origin, such as commonly found for many of the Neogene sediments in East Cape, the porosity is lower and influence of clay minerals more significant. Sandstones are more resistive than siltstones and mudstones. In terms of resistivity models in this study, the most resistive unit is the Tokomaru Sandstone within the Neogene Mangaheia Group (>50 ohm-m). The Neogene mudstone within the Tolaga Group has low resistivity (<10 ohm-m). The Paleocene/Cretaceous units of the Ruatoria and Tinui groups typically have beds of mudstone and sandstone that are 50–100 m thick and show changes from 5 to 10 ohm-m, respectively. The relationship between resistivity and lithology is not simple, so detailed geological information from drill cores would be required to interpret the more subtle variations in resistivity.

Changes in electrical conductivity of the porewater also has a major effect on the bulk resistivity of the subsurface, so, while not the key objective of this study, variations in resistivity can be used to map the extent of salinity in the pore fluids. In thermal springs and geothermal systems, such as might be found at Te Puia, the combination of warm mineralised fluids and alteration of the host rocks to clay minerals produces very low resistivity values (Cumming 2016).

In the following section, we summarise the results from the two areas, using selected resistivity section plots. Appendix 1 contains all of the section plots, with both interpreted and un-interpreted versions.

5.1 Te Puia Springs

The seven profiles across Te Puia Springs show significant changes in resistivity across the area and with changes with depth. Figure 5.1 shows a typical section (Line 600001; see Figure 4.1 for location).

The subsurface is interpreted as four primary layers. Layer 1 is the top 0–20 m. It comprises isolated zones of high resistivity (>100 ohm-m), associated with the sinter, and continuous zones of moderate resistivity (25–100 ohm-m). Layer 2 is a thicker unit that extends from 20 to 100 m depth with resistivity values of between 5 and 25 ohm-m. Layer 3 is slightly higher-resistivity than Layer 2 and extends from 100 to 200 m depth. The basal layer (Layer 4) is typically less than 10 ohm-m and extends to the DOI as determined using the approach of Christensen and Auken (2012). The gaps in the line correspond to houses and powerlines along the road where data are deleted due to interference from these electrical signal sources.

A high-resistivity zone (>100 ohm-m) in Layer 1 is present on the high points in the profile in the centre (sinter) and at the northern end of the line (Cretaceous sandstone). Superimposed on the layered structure are a series of very-low-resistivity zones (<5 ohm-m) that appear to be related to bedding within the units. The lateral changes in this layer may indicate the presence of a fault that vertically offsets the units.

Based on the geological map, the northern end of line 600001 lies on Neogene undifferentiated mudstone and siltstone (Figure 2.2). The high resistivity within Layer 1 indicates that this area is dominated by thin sandstone layers over siltstone. South of Te Puia village, the high resistivity at the surface corresponds with the surface extent of the sinter that forms a prominent ridge 30 m high (Reyes et al. 2010; Pohatu et al. 2010). A resistivity of >200 ohm-m is consistent with the sinter being low-porosity. The sinter is more obvious on line 600601 (Figures 5.2 and 5.3).

Layer 2 is interpreted to be a mudstone unit in the Cretaceous Mokoiwi Formation (Ruatoria Group). The zone of low resistivity (<3 ohm-m) is interpreted to be the thermal fluids that feed the surface springs. The chemistry of the springs indicates that it is dominated by sodium (4500 mg/L) and chloride (7500 mg/L), with minor calcium and bicarbonate components (Reyes et al. 2022; Glover 1968). Based on the composition of the fluids, the resistivity is calculated to be 0.4 ohm-m, and the presence of these fluids in the sediments would reduce the bulk resistivity to less than 3 ohm-m. While the focus of this survey is not the thermal fluids, these may have some influence on the mechanism of slope failure.

Layer 3 is interpreted to be a siltstone layer with a similar low-resistivity zone adjacent to the fault, probably related to thermal fluids. The basal layer (Layer 4) has lower resistivity, indicating more clay-rich sediment.

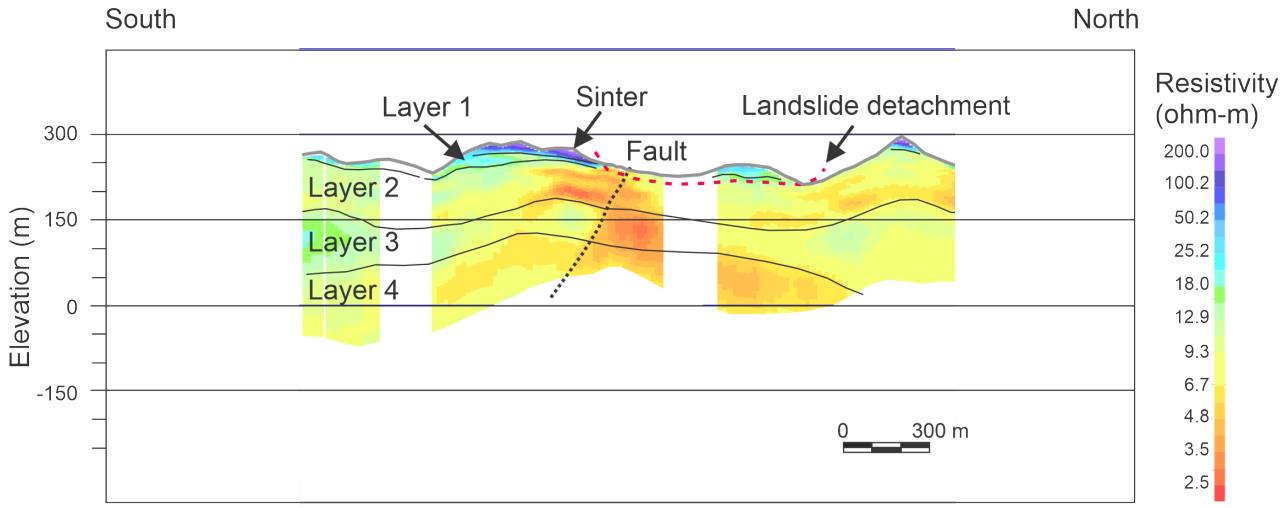

Figure 5.1 Te Puia Springs Line 600001 resistivity section. The section is plotted from south to north. The vertical exaggeration is 2:1. The data below the DOI are masked. The gaps in the profile are associated with buildings and roads that resulted in noisy data being removed from the processing. The shallow landslide detachment surface is shown as a red dashed line.

The tie-line (Line 600601) shows a similar sequence of layers (Figure 5.2). The sinter is seen as a narrow zone of high resistivity at the high point on the section, and we include this as a unit superimposed on Layer 1. Layers 2 and 3 are low-resistivity, and the DOI is reduced to 150 m. The landslide material is likely the upper 20–30 m of moderate resistivity material. The block of high resistivity in the steep hill at the eastern end of the line corresponds to the outcrop of Neogene Tokomaru Sandstone (Mmk) within the Mangaheia Group. Two mapped faults are seen extending to depth on the eastern side of the sandstone outcrop and delineate the contact with undifferentiated Neogene siltstone and mudstone (MI). We map two faults in the AEM data and interpret the dips to be vertical or steeply west-dipping. Only one fault is identified in the QMAP sheet (Mazengarb and Speden 2000).

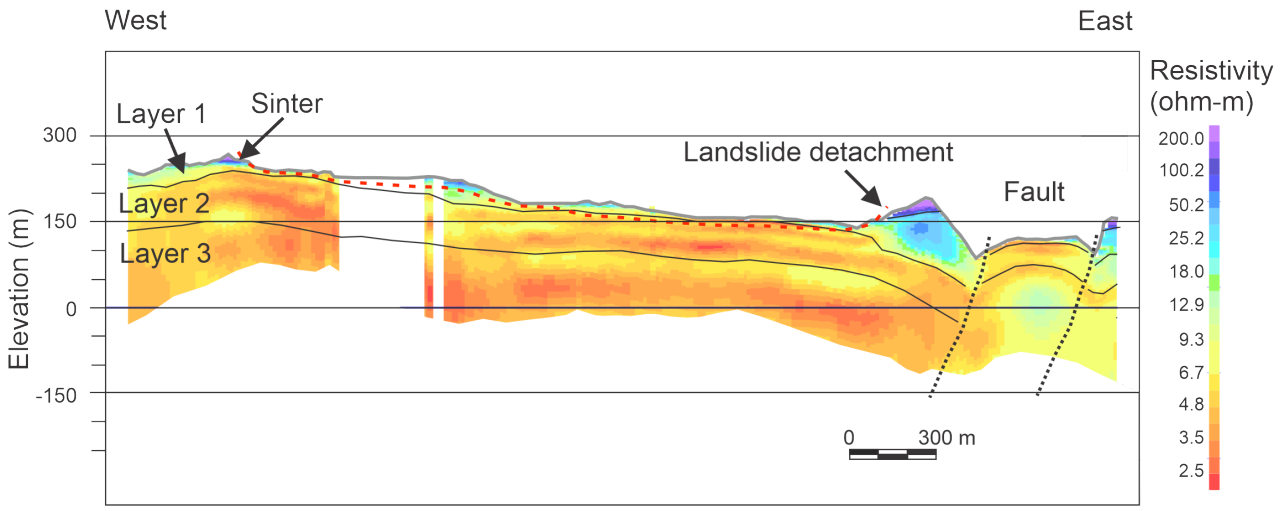

Figure 5.2 Te Puia Springs Line 600601 resistivity section. The section is plotted from west to east. The vertical exaggeration is 2:1. The data below the DOI are masked. The interpreted section shows the primary layers 1–3. The gaps in the profile are associated with buildings and roads that resulted in noisy data being removed from the processing. The shallow landslide detachment surface is shown as a red dashed line.

The other five lines show the same layering to depths of 250–300 m. The contact between the shallow Cretaceous units and Quaternary landslide material is subtle, but, on the northeastern edge, the resistive Cretaceous Taitai Sandstone (Ruatoria Group) is a thin layer that is truncated sharply by the edge of the landslide (Figure 5.3).

Previous interpretations of deeper AMT/MT data showed a thick Quaternary layer, but this is likely to be poorly resolved by the ground-based geophysics (Zygadlo et al. 2015). The AEM data indicate that the landslide unit is thin (<50 m) and that the layered Cretaceous units are laterally continuous under the landslide. The eastern edge of the landslide probably covers a series of faults in the bedrock where Cretaceous units are juxtaposed against Neogene units. The blocks of high-resistivity Neogene Tokomaru Sandstone may be either entrained within the landslide or be a block in intact bedrock that has forced the landslide deposit to pass around its flanks (Figure 5.2).

The thermal fluids associated with the surface springs appear as zones of very low resistivity (<3 ohm-m) that are confined to an area near a potential fault zone through the Cretaceous rocks in the southwest area of the landslide.

Figure 5.3 shows a view of the Te Puia geophysical transects and the outlines of the source and deposit zones of the landslide (Figure 2.2). The northern edge of the landslide is difficult to map with the SkyTEM resistivity data, but there is a thin layer of high resistivity at the surface on the northern end of each section line. This layer is less than 10 m thick but is a continuous layer outside the limits of the landslide, not present in the landslide source zone, present as isolated blocks distributed through the deposit zone. This distribution of shallow resistive rock is consistent with blocks of material being moved from the source region into the deposit region on a shallow glide-plane.

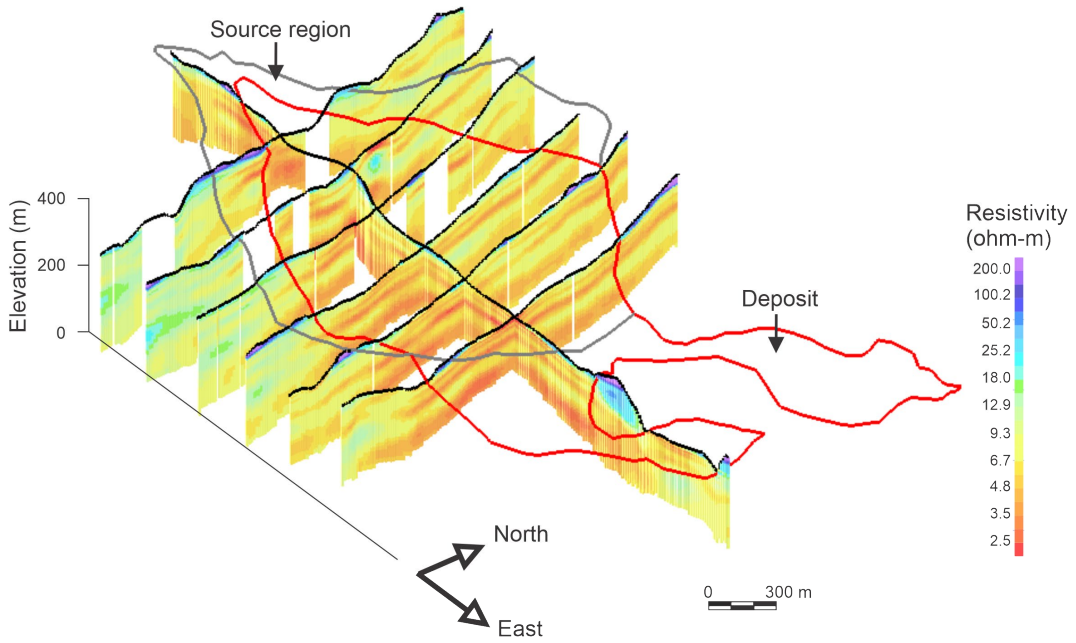

Figure 5.3 Three-dimensional view of Te Puia Springs showing the SkyTEM sections and mapped extents of the landslide source (grey) and deposit (red) regions. The view is to the northwest. The vertical exaggeration is 2:1.

5.2 Mangahauini Gorge

The AEM survey over the landslide in the Mangahauini Gorge focused on the large slope along the western side of the river (Figures 2.3, 2.5 and 4.2). The survey comprised four lines parallel to the slope and one tie-line perpendicular to the slope. Figure 2.3 shows the extensive long-lived landslide deposit of Mangahauini Landslide and the more recent 2023 landslide that re-mobilised some of the deposit and blocked the river. The tie-line crosses over Mangahauini River and extends up the eastern side of the gorge over another landslide deposit (Figure 4.2). The lines parallel to the river extend across other mapped landslides to the south and north of the main slope.

The five profiles across the Mangahauini Gorge show significant changes in resistivity across the area and with changes in depth. Figure 5.4 shows a typical section (Line 700401; see Figure 4.2 for location). All of the cross-sections are shown in Appendix 1.

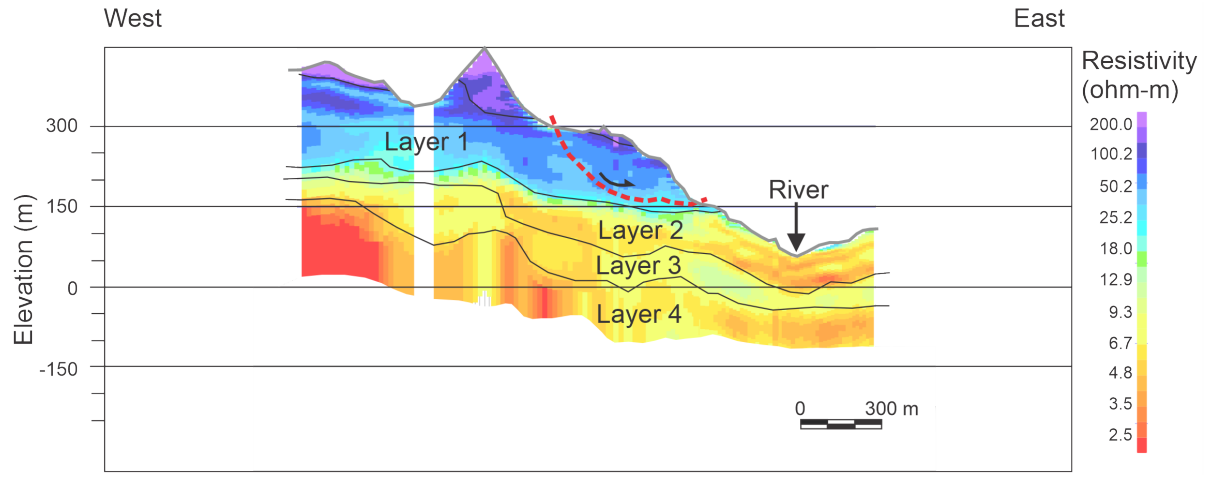

Figure 5.4 Mangahauini Line 700401 resistivity section. The section is plotted from west to east. The vertical exaggeration is 2:1. The data below the DOI are masked. The interpreted section shows the primary layers 1–4 with the interpreted deep-seated failure surface indicated as the dashed red line. The arrow shows the sense of rotation of the block.

The same layered interpretation adopted at Te Puia Springs has been used on the Mangahauini lines. Layer 1 is a highly resistive unit corresponding to the Neogene Tokomaru Sandstone (Mmk : Mangaheia Group). The Areoma Sandstone (MIr : Tolaga Group) is also present in the area and likely forms similar high-resistivity layers. The ridge tops show resistivity values as high as 200 ohm-m. The unit is at least 250 m thick and dips to the east. The section in Figure 5.4 shows some vertical variations within Layer 1 on the order of 50 m thickness, possibly related to alternations between more resistive sandstones and less resistive siltstones.

The second layer is a low-resistivity unit (5–8 ohm-m) within the undifferentiated Neogene mudstone and siltstone (MI). There is some evidence near the river of thinner bedding (<10 m). Quaternary alluvial deposits sit directly on Neogene siltstone along the banks of the river. While the resistivity of Layer 2 is similar at Mangahauini and Te Puia, the geological units at Te Puia are older (Figure 5.2).

Layer 3 is similar to Layer 2 but has a more moderate resistivity of 15–30 ohm-m.

The basal unit is Layer 4 and resistivity decreases to less than 4 ohm-m, indicating that the lithology is dominantly mudstone.

The tie-line (700401) is close to the boundary between the more resistive Areoma Sandstone (MIr : Tolaga Group) in the north (Layer 1) and the moderate-resistivity siltstone and mudstone (Layers 2–4) in the south (Undifferentiated MI: Tolaga Group). A major stream cuts down through the Areoma Sandstone unit north of the tie-line (see Figures 2.3 and 4.2) and forms the northern boundary of Mangahauini Landslide. The 2023 landslide has been developed in the siltstone and mudstone formations that lie in the southern part of the surveyed area.

The source area for the main block of the landslide lies within the resistive sandstone units. We have interpreted a change in resistivity within Layer 1 in the landslide deposit adjacent to the source region to be a detachment (i.e. landslide failure) surface. The depth to the detachment could be 150 m at its deepest extent. The detached block shows evidence of rotation in the resistivity profile. This rotation results in the detachment being exposed at the base of the slope. The eastern slopes of the rotated block are steep, and secondary landslides have deposited material into the river valley (Figure 5.4). Near the river, 5–10 m of Quaternary cover lies on top of the Neogene siltstone, and this juxtaposition of units may represent landslide deposits. These deposits could be derived from either side of the valley.

Figure 5.5 shows a three-dimensional view of the dataset showing the extents of the landslide source region and three main blocks identified as the deposits. Figure 5.5a shows the interpretation of the detachment surface in three dimensions, highlighting its complex geometry.

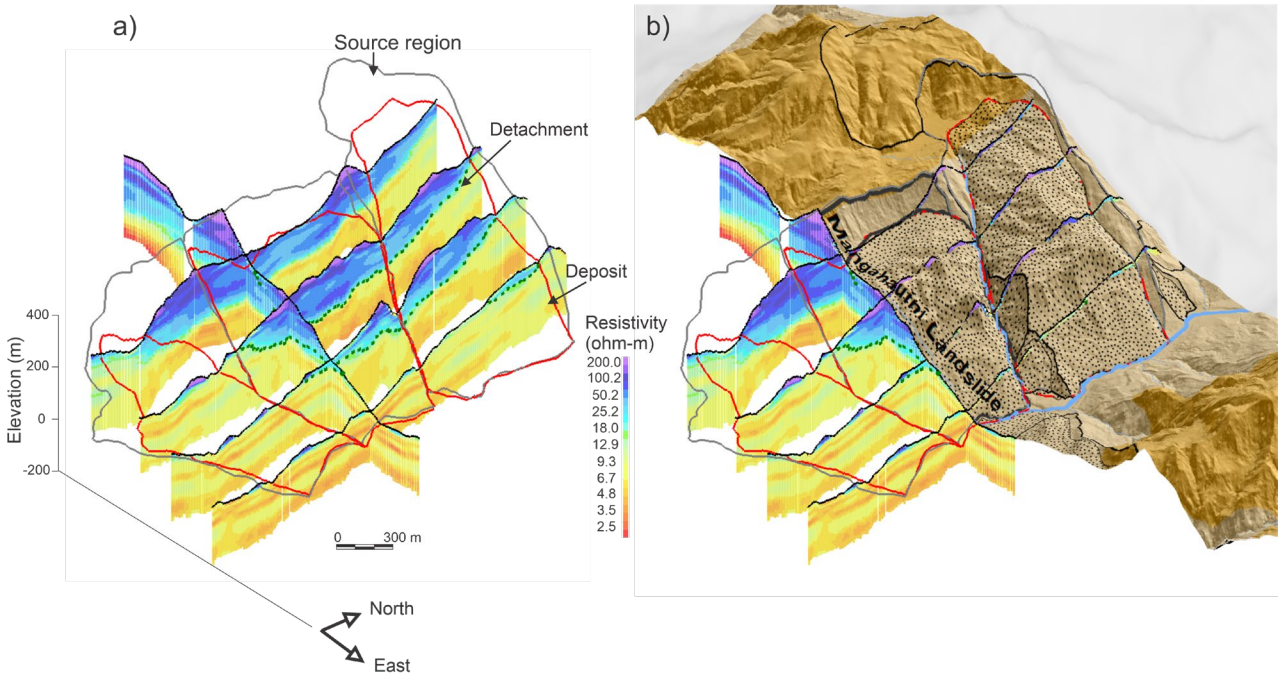

Figure 5.5 Three-dimensional view of the western side of Mangahauini Gorge, showing the SkyTEM sections and mapped extents of the landslide source regions (grey), deposit areas (red) and interpreted detachment surface (green dashed line). The Mangahauini slide is the landslide in the centre. The view is to the northwest. The vertical exaggeration is 2:1. (a) Three-dimensional view of SkyTEM sections. (b) Surface geology map shown draped over the topography in the northern half of the survey.

The area of Mangahauini Landslide is dominated by the higher-resistivity layers of the Neogene Tokomaru Sandstone (Mangaheia Group) and Areoma Sandstone (Tolaga Group). The adjacent smaller landslide source area to the south is on the boundary between the Areoma Sandstone and underlying mudstones (Tolaga Group). The upper area of this slide shows slightly higher resistivities. The 2023 landslide (not shown on Figure 5.5) is located entirely in the low-resistivity region of the Neogene siltstones (Tolaga Group) or Quaternary cover.

The creek that drains into Mangahauini River in the northern part of the survey area has a marked linear pattern. There is some evidence for a truncation of layering in the SkyTEM section that runs close to the river along the eastern edge of the survey (see Figure 5.5a). We interpret the linear character of the creek, as well as the offset in the bedding in the SkyTEM resistivity sections, to indicate that the creek may be fault-controlled.

6.0 Discussion

The SkyTEM survey was an efficient way of imaging the broadscale features of the Te Puia Springs and Mangahauini landslides. The survey was completed in a single flight during the groundwater-mapping project in Waiapu and Uawa. The resistivity structure of Cretaceous and Neogene rocks and younger surficial materials showed clear indications of layering and vertical changes in resistivity. Faulting was clearly seen in the Te Puia Springs survey, with some indication of a fault in Mangahauini Gorge.

The fine details (<20 m depth) of the landslides at both Te Puia Springs and Mangahauini are not adequately captured by the airborne electromagnetic system. Increasing vertical resolution in the top 20 m would require a smaller loop, denser grid of flight lines and flying closer to the ground surface to delineate fine surficial landslide details. Alternatively, given the strong resistivity variations seen across these landslides, ground-based geophysical methods such as Electrical Resistivity Tomography (ERT) or ground TEM may be more effective. Such methods would help to map even greater subsurface detail in these types of large, soft-rock landslides, if terrain and safety considerations make such surveys feasible – this is probably more feasible at Te Puia than over the steep topography of Mangahauini Gorge. Resistivity (ERT) surveys have been used successfully elsewhere in the country on different landslide types.

At Te Puia Springs, the highly saline thermal waters were imaged to depths of 150 m, and faulting and sedimentary layers appear to influence the distribution of the low-resistivity zones associated with the saline fluids. The lines that crossed the prominent sinter at the surface showed that it was highly resistive and hence mappable. While not the focus of the current research, the results of this work provide motivation for considering AEM as a technique for mapping low-temperature geothermal systems.

7.0 Conclusions and Recommendations

For the landslide sites specifically, these data help to support hypotheses about the origin of the landslides and to define the size and limits of the landslides.

For the Te Puia Springs case study, the data support a view that the landslide unit is relatively thin (<50 m), sliding above the Cretaceous rocks, and that the landslide has entrained and translocated blocks of more resistive rock. The data also help to confirm the boundaries of the landslide that were identified from geomorphological mapping.

For the Mangahauini case study, the data help to show the wider slope-stability context for the river-blocking landslide that was generated in 2023 following the extreme weather events, indicating that the landslide that blocked the river is part of a much larger area of slope instability.

More broadly, the study shows that the SkyTEM technology can be useful for getting rapid and safe assessments of landslide geometry and understanding the geological context of the landslides. This in turn could be useful for supporting decisions around landslide hazard- and risk-management following extreme events. In addition, the technology can also support longer-term planning for areas affected by active or dormant landslides.

The airborne surveying technology (SkyTEM) collects data over a range of depth intervals from about 10 m to 200–300 m below ground surface. Most landslides involve material in the top 100 m or shallower. The shallower parts of the landslide in the current project may not be captured with sufficient detail using the SkyTEM survey, but the deeper parts of the landslide were mapped. Covering a large landslide in detail would be logistically challenging with any method. However, as noted above, different survey configurations that are customised for the collection of higher-resolution surficial data would likely help to capture more relevant detail of the surficial materials in localised areas.

A key advantage of the airborne electromagnetic surveys, using helicopter-deployed TEM, is that large areas of ground can be surveyed rapidly without the added dangers of personnel needing to spend time on potentially dangerous landslides or steep, difficult terrain. In this way, the study demonstrated that SkyTEM or similar airborne electromagnetic surveys could be a practical solution for rapid assessment of landslide size and geological conditions.

Another lesson learned was that any future surveys should ensure that the flight lines used are extended farther beyond the target features to ensure that the landslide boundaries can be identified. In this study, there was some doubt about where the landslide boundaries were when planning the flight lines. In retrospect, the flight lines should have been extended slightly further in all directions. This could have been done with minimal extra cost.

8.0 Acknowledgements

The collection of the SkyTEM data was funded by the Ministry of Business, Innovation & Employment (MBIE) through a Cyclone Gabrielle response grant to GNS Science (February 2024) to support work by Gisborne District Council (Grant number GNS2332). The processing, interpretation and reporting were supported by an MBIE Strategic Science Investment Fund to Earth Sciences New Zealand (contract C05X1702). Murry Cave from Gisborne District Council is thanked for providing valuable feedback on the project design and initial interpretation of the data. Input from Caleb Gasston and Rob Haskell of LDE Ltd provided some additional comments on the geology of the area. Ben Pasco from Aqua Intel Aotearoa (Kānoa REDIU) facilitated the surveying by SkyTEM Australia Pty Ltd during its groundwater survey in Tairāwhiti Gisborne. SkyTEM Australia Pty Ltd undertook the survey efficiently and provided the data in a timely manner. This report has benefitted from reviews by Sally Dellow and Vaughan Stagpoole.

9.0 References

Auken E, Christiansen AV, Westergaard JH, Kirkegaard C, Foged N, Viezzoli A. 2009. An integrated processing scheme for high-resolution airborne electromagnetic surveys, the SkyTEM system. *Exploration Geophysics*. 40(2):184–192. https://doi.org/10.1071/EG08128

Auken E, Christiansen AV, Kirkegaard C, Fiandaca G, Schamper C, Behroozmand AA, Binley A, Nielsen E, Effersø F, Christensen NB, et al. 2015. An overview of a highly versatile forward and stable inverse algorithm for airborne, ground-based and borehole electromagnetic and electric data. *Exploration Geophysics*. 46(3):223–235. https://doi.org/10.1071/EG13097

Bruce ZRV. 2022. Version 1 of the New Zealand landslide fatalities database, 1760–2020. Lower Hutt (NZ): GNS Science. 114 p. (GNS Science report; 2021/38). https://doi.org/10.21420/SW43-TJ28

Christiansen AV, Auken E. 2012. A global measure for depth of investigation. *Geophysics*. 77(4):WB171–WB177. https://doi.org/10.1190/geo2011-0393.1

Cumming W. 2016. Geophysics and resource conceptual models in geothermal exploration and development. In: DiPippo R, editor. *Geothermal Power Generation*. Duxford (GB): Woodhead Publishing. p. 33–75. https://doi.org/10.1016/B978-0-08-100337-4.00003-6

Gibb JG. 1981. Coastal hazard mapping as a planning technique for Waiapu County, East Coast, North Island, New Zealand: He ripoata whakature mo nga whenua papa-a-tai o te rohe o te kaunihera o Waiapu-Tairawhiti. Wellington (NZ): Ministry of Works & Development. 63 p. (Water & Soil technical publication; 21).

Glover RB. 1968. Chemical analyses of and brief comments on miscellaneous mineral waters including Awakeri, Tarawera, Puketitiri, Te Puia, Waimata Valley, Gisborne, Morere, Raukawa, Wallingford, Weber, Mataroa and the Wanganui. 14 p. + 1 fig. Located at: Earth Sciences New Zealand, Lower Hutt, NZ; Geothermal circular RBG 23.

Hastings District Council. 2024 Dec. Cyclone Gabrielle updates: roading recovery update – December 2024. Hastings (NZ): Hastings District Council; [accessed 2025 Feb 19]. https://mailchi.mp/5f6b6905222a/roading-recovery-update-december

Heise W, Caldwell TG, Bertrand EA, Hill GJ, Bennie SL, Ogawa Y. 2013. Changes in electrical resistivity track changes in tectonic plate coupling. *Geophysical Research Letters*. 40(19):5029–5033. https://doi.org/10.1002/grl.50959

Impact Consulting Ltd. 2018. Ngāti Porou Hauora community facilities redevelopment: feasibility investigations for hospital and community facilities redevelopment, Te Puia Springs, East Cape, NZ. Wellington (NZ): Impact Consulting. 140 p. Prepared for Ngāti Porou Hauora.

Isacsson U, Persson L, Smith CA. 2021. Airborne geophysical investigations for landslide risk investigation along the Ångerman River, central Sweden. *IOP Conference Series: Earth and Environmental Science*. 710(1):012009. https://doi.org/10.1088/1755-1315/710/1/012009

Laing ACM. 1972. Alliance Te Puia No. 1 well. Located at: Ministry of Business, Innovation & Employment, Wellington, NZ. 183 p. + 12 enclosures. New Zealand Unpublished Petroleum Report 257.

Lin AF, Zorn C, Wotherspoon L, Robinson TR, Pelmard J. 2025. Prediction of road blockages caused by rainfall-induced landslides. *New Zealand Journal of Geology and Geophysics*. 68(5):983–999. https://doi.org/10.1080/00288306.2025.2454565

[LINZ] Toitū Te Whenua Land Information New Zealand. 2021. Gisborne LiDAR 1m DEM (2018–2020). Wellington (NZ): LINZ; [updated 2025 Sep 9; accessed 2025 Dec]. https://data.linz.govt.nz/layer/105614-gisborne-lidar-1m-dem-2018-2020/

Marden M, Betts H, Arnold G, Hambling R. 2008. Gully erosion and sediment load: Waipaoa, Waiapu and Uawa rivers, eastern North Island, New Zealand. In: Schmidt J, Cochrane T, Phillips C, Elliot S, Davies T, Basher L, editors. *Sediment dynamics in changing environments*. Wallingford (GB): International Association of Hydrological Sciences. p. 339–350. (IAHS publication; 325).

Mazengarb C, Speden IG, compilers. 2000. Geology of the Raukumara area [map]. Lower Hutt (NZ): Institute of Geological & Nuclear Sciences Limited. 60 p. + 1 map, scale 1:250,000. (Institute of Geological & Nuclear Sciences 1:250,000 geological map; 6).

[MBIE] Ministry of Business, Innovation & Employment. 2012. Review of the Maui pipeline outage of October 2011. Wellington (NZ): MBIE; [accessed 2025 Dec]. https://www.mbie.govt.nz/assets/52fe4c4bd3/review-maui-pipeline-outage-october-2011.pdf

McMillan A, Dymond J, Jolly B, Shepherd J, Sutherland A. 2023. Rapid assessment of land damage – Cyclone Gabrielle. Lincoln (NZ): Manaaki Whenua Landcare Research. 28 p. Contract Report LC4292. Prepared for the Ministry for the Environment. https://environment.govt.nz/assets/Rapid-assessment-of-land-damage-Cyclone-Gabrielle-Manaaki-Whenua-Landcare-Research-report.pdf

Oborn LE. 1980. Slope instability at Te Puia Springs. Lower Hutt (NZ): New Zealand Geological Survey. 10 p. Report EG 351.

Page M, Trustrum N, Gomez B. 2000. Implications of a century of anthropogenic erosion for future land use in the Gisborne-East Coast region of New Zealand. *New Zealand Geographer*. 56(2):13–24. https://doi.org/10.1111/j.1745-7939.2000.tb01571.x

Palacky GJ. 1987. Resistivity characteristics of geologic targets. In: Nabighian MN, editor. *Electromagnetic methods in applied geophysics. Volume 1: theory*. Tulsa (OK): Society of Exploration Geophysicists. p. 53–130. https://doi.org/10.1190/1.9781560802631.ch3

Pohatu P, Warmenhoven T, Rae A, Bradshaw D. 2010. Low enthalpy geothermal energy resources for rural Māori communities – Te Puia Springs, East Coast, North Island New Zealand. In: *Proceedings of the World Geothermal Congress 2010*; 2010 Apr 25–30; Bali, Indonesia. Bonn (DE): International Geothermal Association. 6 p.

Rawlinson ZJ, Foged N, Westerhoff RS, Kellett RL. 2021. Hawke's Bay 3D Aquifer Mapping Project: Heretaunga Plains SkyTEM data processing and resistivity models. Wairakei (NZ): GNS Science. 90 p. Consultancy Report 2021/93. Prepared for Hawke's Bay Regional Council.

Reyes AG, Christenson BW, Faure K. 2010. Sources of solutes and heat in low-enthalpy mineral waters and their relation to tectonic setting, New Zealand. *Journal of Volcanology and Geothermal Research.* 192(3–4):117–141. https://doi.org/10.1016/j.jvolgeores.2010.02.015

Reyes AG, Ellis SM, Christenson BW, Henrys S. 2022. Fluid flowrates and compositions and water–rock interaction in the Hikurangi margin forearc, New Zealand. *Chemical Geology*. 614:121169. https://doi.org/10.1016/j.chemgeo.2022.121169

Reynolds JM. 2011. An introduction to applied and environmental geophysics. 2nd ed. Chichester (GB): Wiley-Blackwell. 696 p.

Saul G, Anderson C. 2019. Kaikoura earthquake 2016: an outline of the geotechnical effort to reopen the coastal highway and railway corridor. In: Silvestri F, Moraci N, editors. *Earthquake geotechnical engineering for protection and development of environment and constructions: proceedings of the 7th International Conference on Earthquake Geotechnical Engineering; 2019 Jun 17–20; Rome, Italy*. London (GB): CRC Press. p. 4890–4897.

Singeisen C, Massey C, Wolter A, Kellett R, Bloom C, Stahl T, Gasston C, Jones K. 2022. Mechanisms of rock slope failures triggered by the 2016 M_W 7.8 Kaikōura earthquake and implications for landslide susceptibility. *Geomorphology*. 415:108386. https://doi.org/10.1016/j.geomorph.2022.108386

SkyTEM Australia Pty Ltd. 2024. SkyTEM helicopter EM survey: Gisborne AEM survey, New Zealand. Malaga (AU): SkyTEM Australia Pty Ltd. 61 p. Prepared for GNS Science.

Sørensen K, Auken E. 2004. SkyTEM – a new high-resolution helicopter transient electromagnetic system. *Exploration Geophysics*. 35(3):194–202. https://doi.org/10.1071/EG04194

Wolter A, Rosser BJ, Cave M, Morgenstern R, Farr J, Massey CI. 2023. Mangahauini / Tokomaru Bay landslide dam: initial scientific observations, survey results and breach inundation modelling. Lower Hutt (NZ): GNS Science. 21 p. (GNS Science report; 2023/11). https://doi.org/10.21420/SENN-CB35

Zygadlo M, Rae AJ, Reeves R, Wallin E, Pohatu P. 2015. Te Puia Springs, East Coast, New Zealand, low enthalpy geothermal review. Lower Hutt (NZ): GNS Science. 41 p. (GNS Science report; 2015/04).

This page left intentionally blank.

APPENDICES

This page left intentionally blank.

APPENDIX 1 SkyTEM Profiles

A1.1 Te Puia Survey

This appendix contains the interpreted and un-interpreted sections from each of the flight lines from Te Puia Springs.

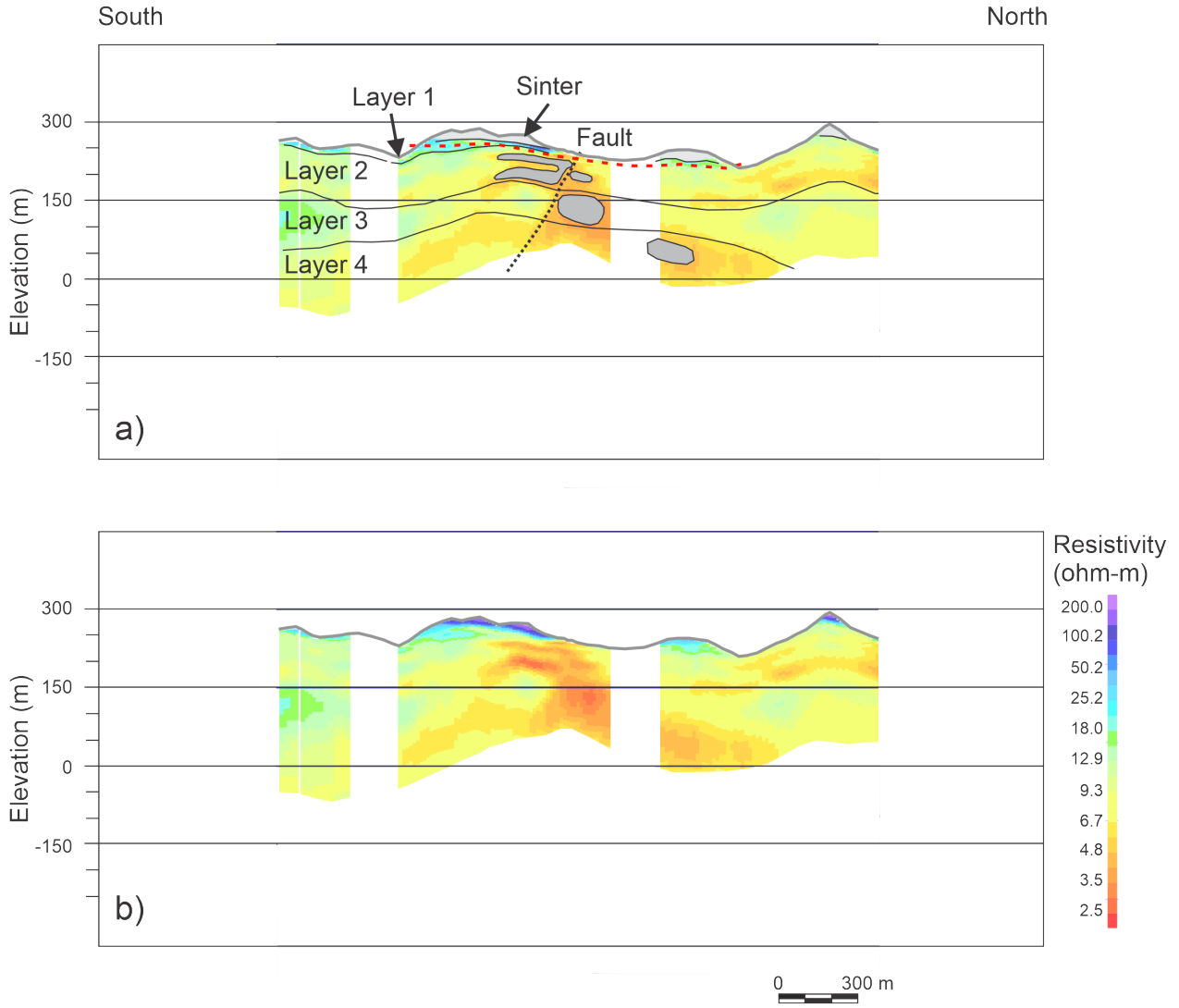

Figure A1.1 Te Puia Springs Line 600001 resistivity section. The section is plotted from south to north. The vertical exaggeration is 2:1. The data below the DOI are masked. (a) Interpreted section showing the primary layers 1–4, the zone of high resistivity at the surface (light shading) and the zones of low resistivity (medium shading). (b) Section without interpretation. The gaps in the profile are associated with buildings and roads that resulted in noisy data being removed from the processing.

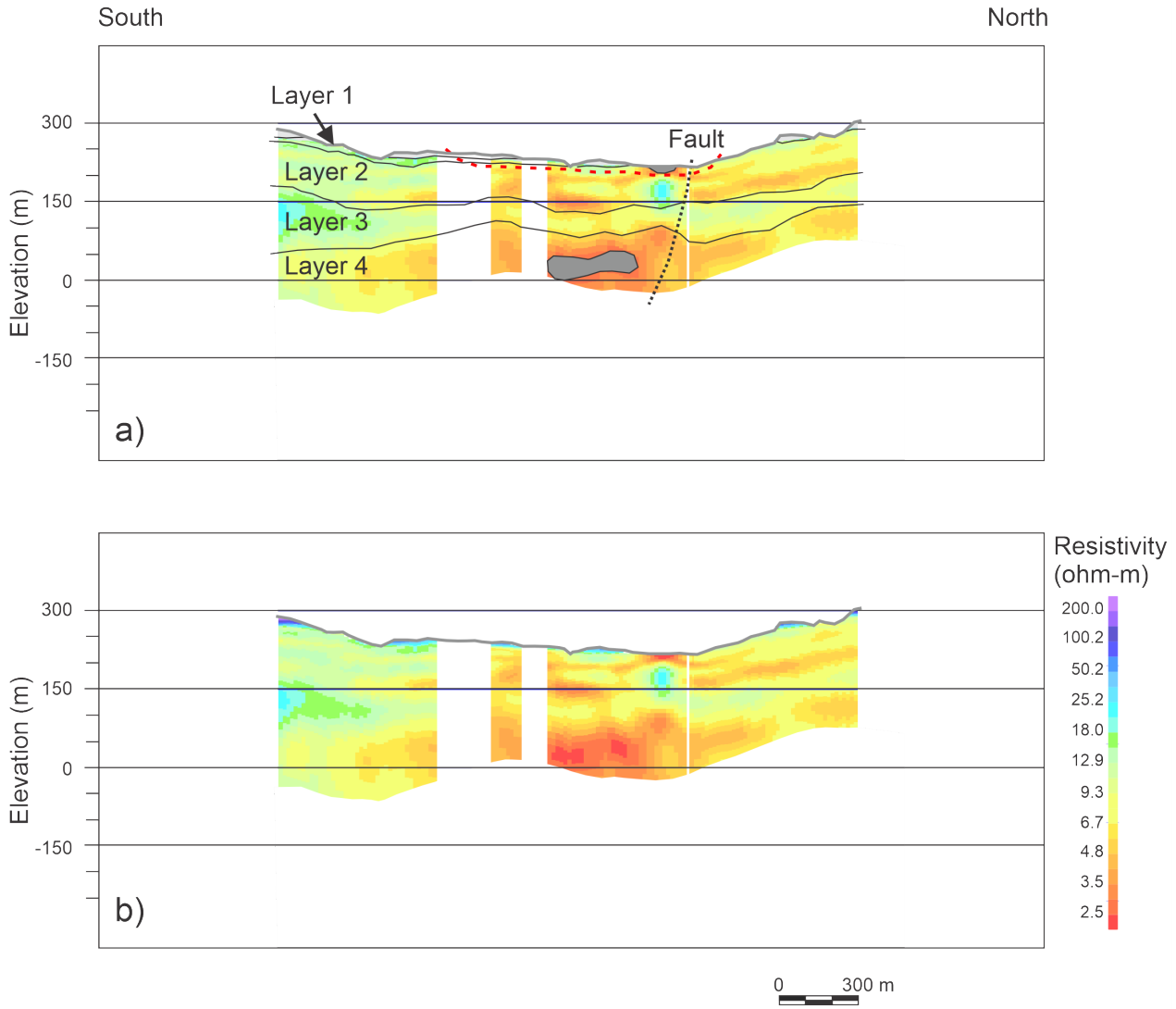

Figure A1.2 Te Puia Springs Line 600101 resistivity section. The section is plotted from south to north. The vertical exaggeration is 2:1. The data below the DOI are masked. (a) Interpreted section showing the primary layers 1–4, the zone of high resistivity at the surface (light shading) and the zones of low resistivity (medium shading). (b) Section without interpretation. The gaps in the profile are associated with buildings and roads that resulted in noisy data being removed from the processing.

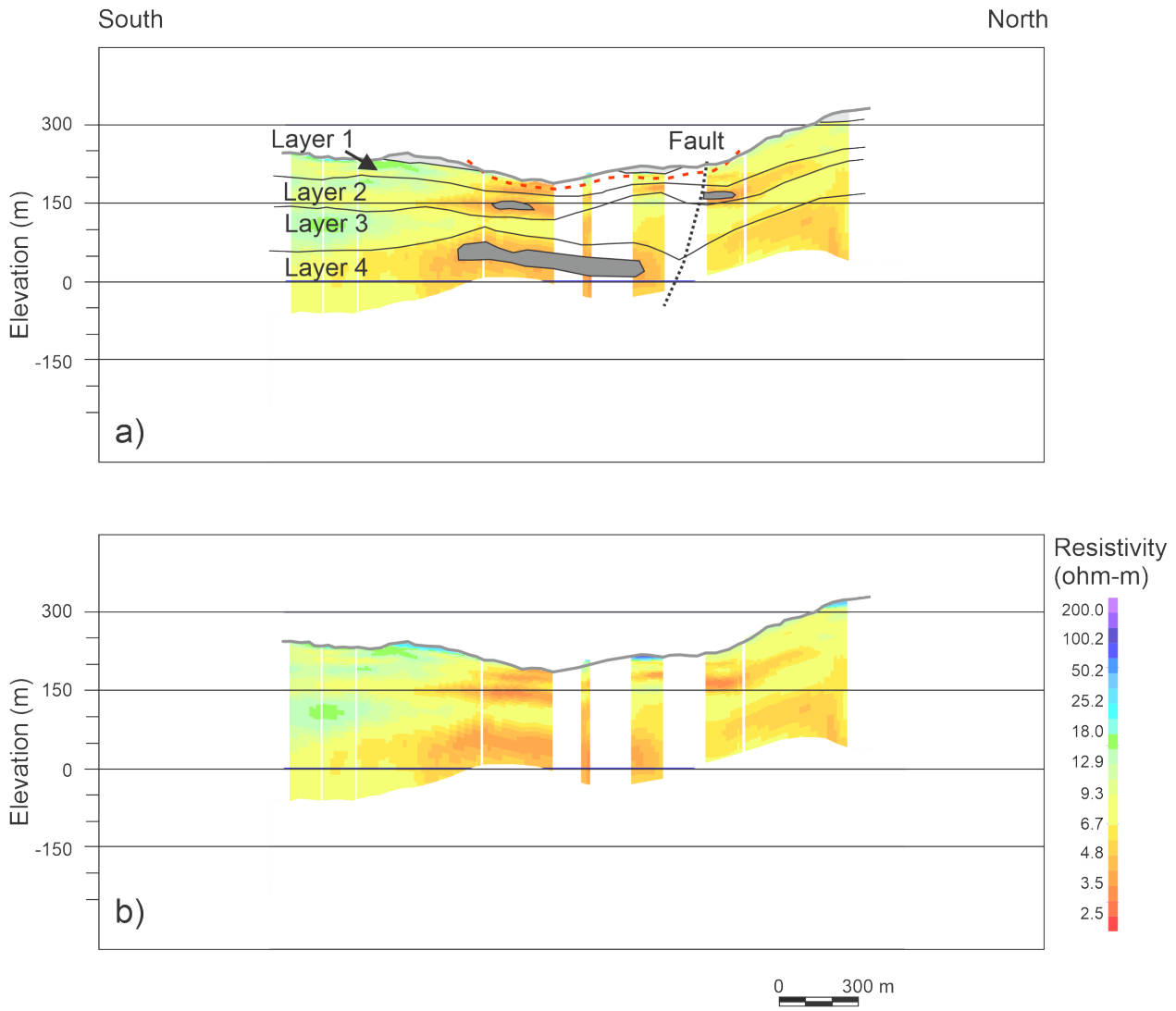

Figure A1.3 Te Puia Springs Line 600201 resistivity section. The section is plotted from south to north. The vertical exaggeration is 2:1. The data below the DOI are masked. (a) Interpreted section showing the primary layers 1–4, the zone of high resistivity at the surface (light shading) and the zones of low resistivity (medium shading). (b) Section without interpretation. The gaps in the profile are associated with buildings and roads that resulted in noisy data being removed from the processing.

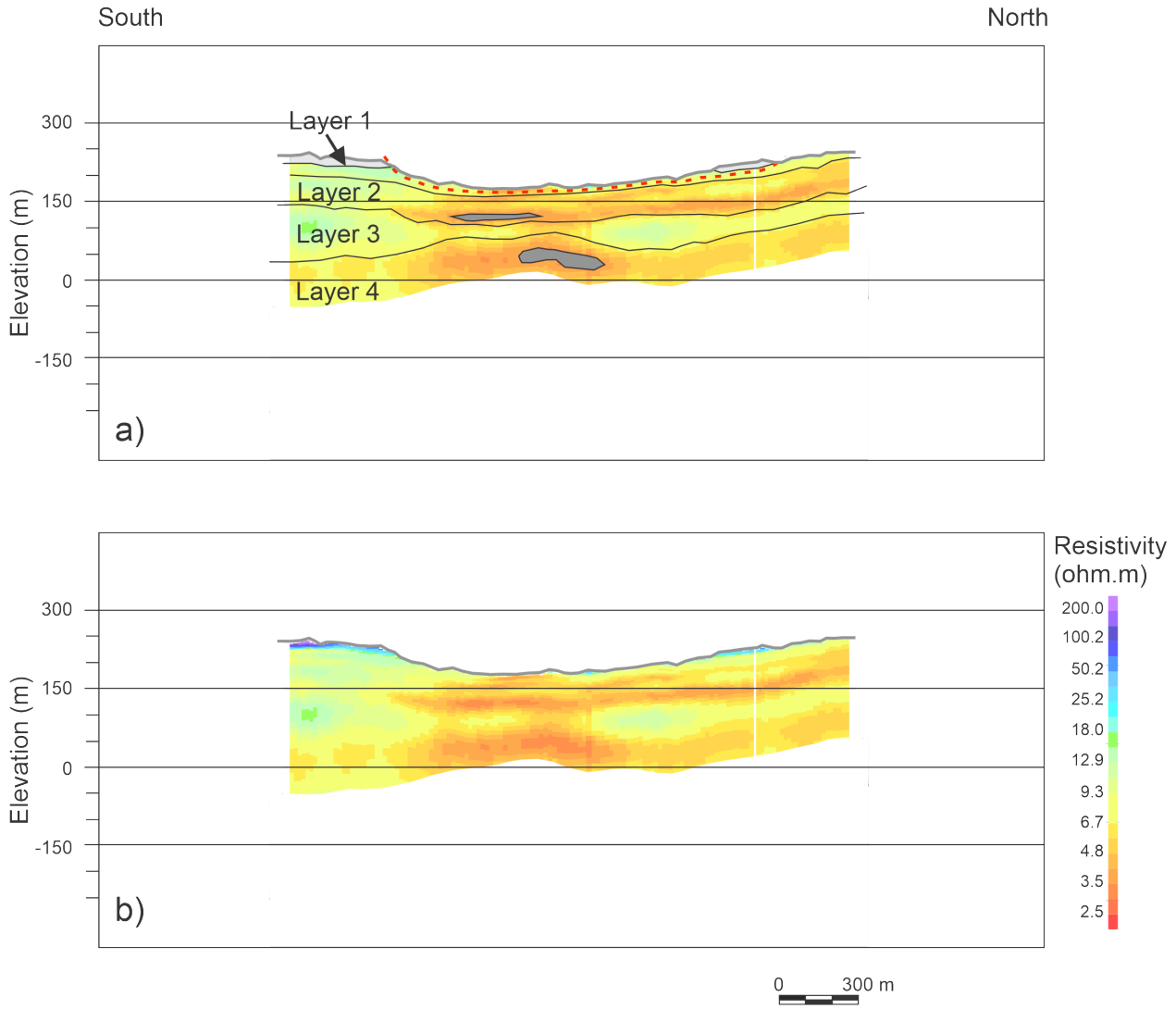

Figure A1.4 Te Puia Springs Line 600301 resistivity section. The section is plotted from south to north. The vertical exaggeration is 2:1. The data below the DOI are masked. (a) Interpreted section showing the primary layers 1–4, the zone of high resistivity at the surface (light shading) and the zones of low resistivity (medium shading). (b) Section without interpretation. The gaps in the profile are associated with buildings and roads that resulted in noisy data being removed from the processing.

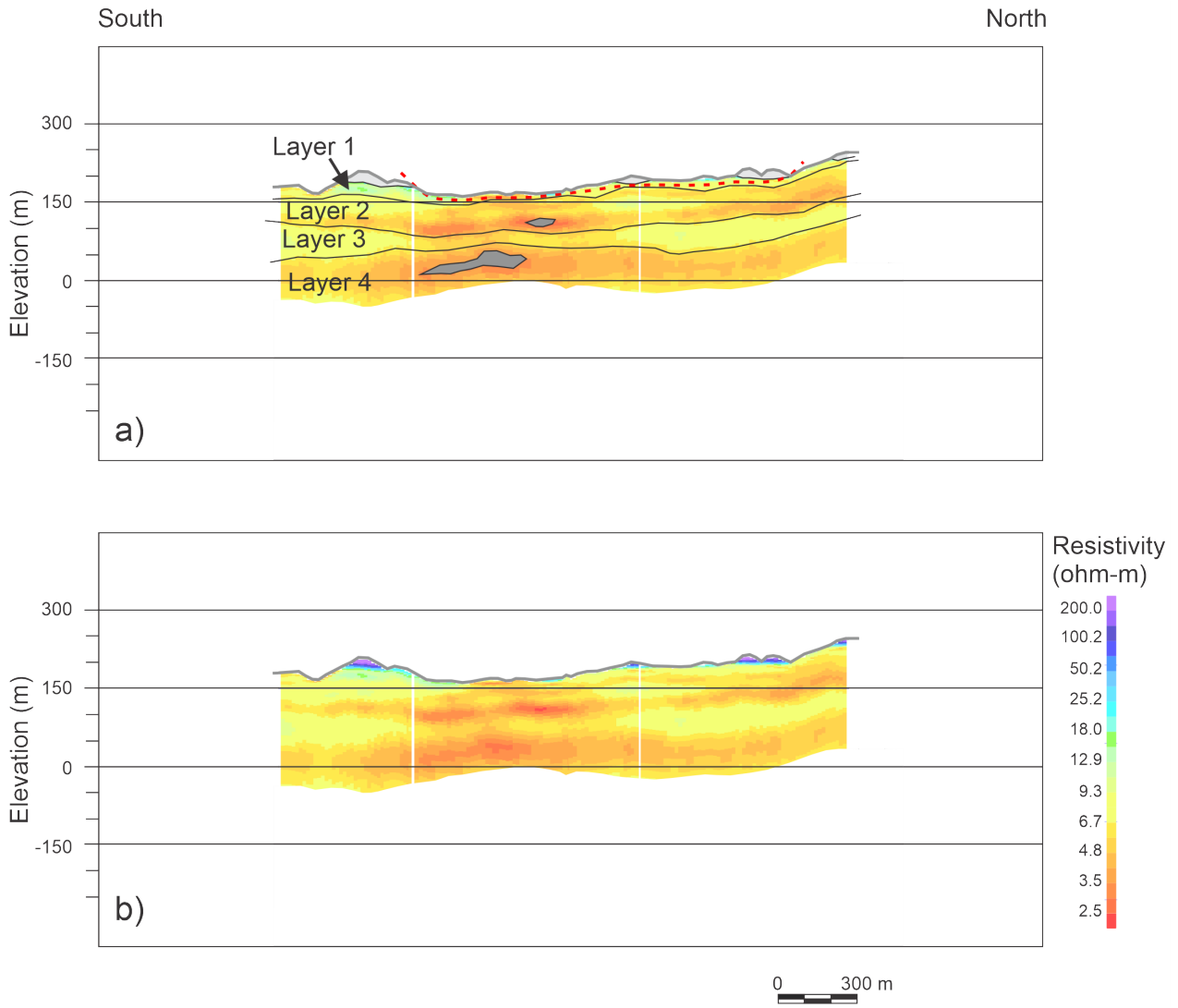

Figure A1.5 Te Puia Springs Line 600401 resistivity section. The section is plotted from south to north. The vertical exaggeration is 2:1. The data below the DOI are masked. (a) Interpreted section showing the primary layers 1–4, the zone of high resistivity at the surface (light shading) and the zones of low resistivity (medium shading). (b) Section without interpretation. The gaps in the profile are associated with buildings and roads that resulted in noisy data being removed from the processing.

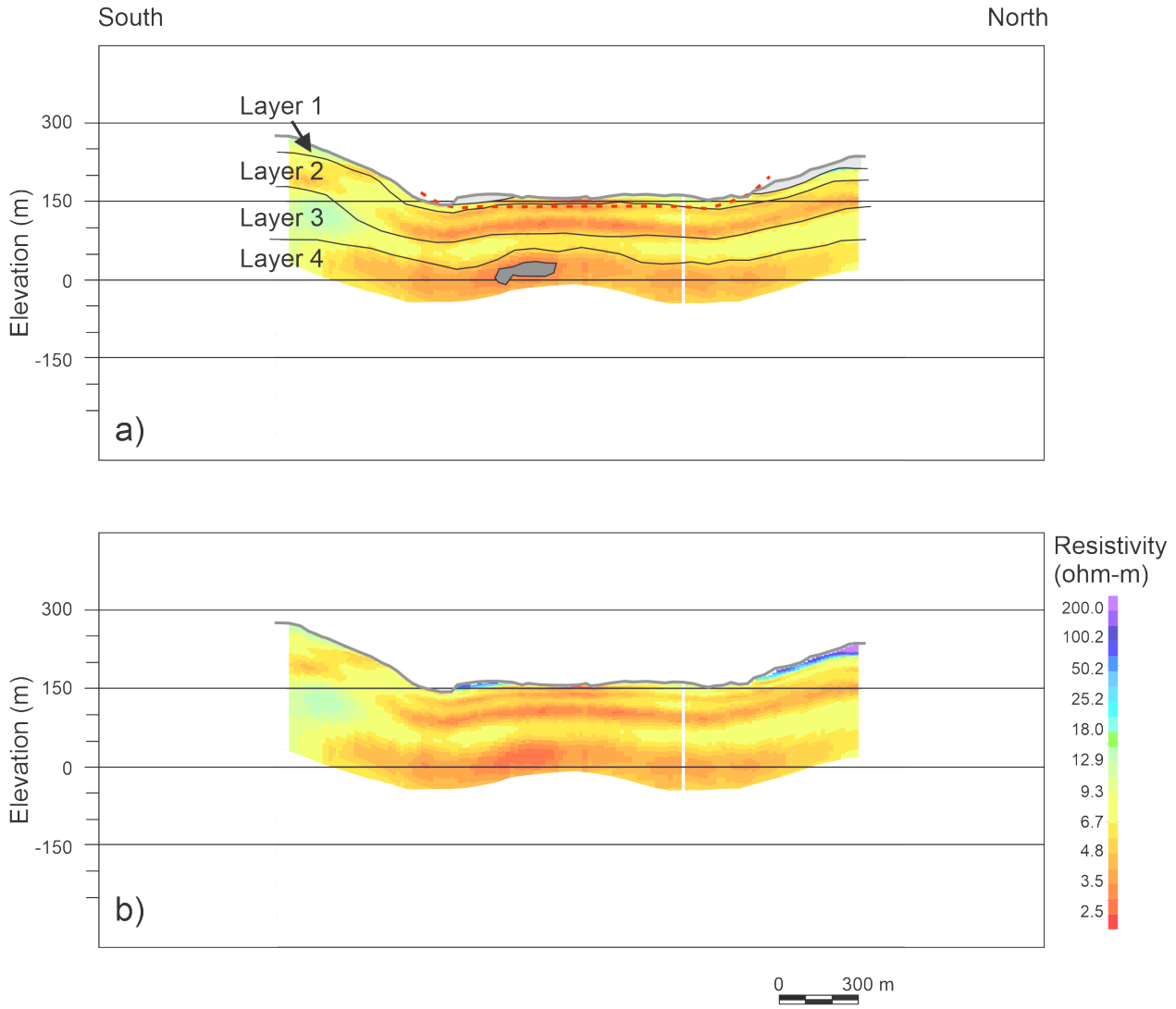

Figure A1.6 Te Puia Springs Line 600501 resistivity section. The section is plotted from south to north. The vertical exaggeration is 2:1. The data below the DOI are masked. (a) Interpreted section showing the primary layers 1–4, the zone of high resistivity at the surface (light shading) and the zones of low resistivity (medium shading). (b) Section without interpretation. The gaps in the profile are associated with buildings and roads that resulted in noisy data being removed from the processing.

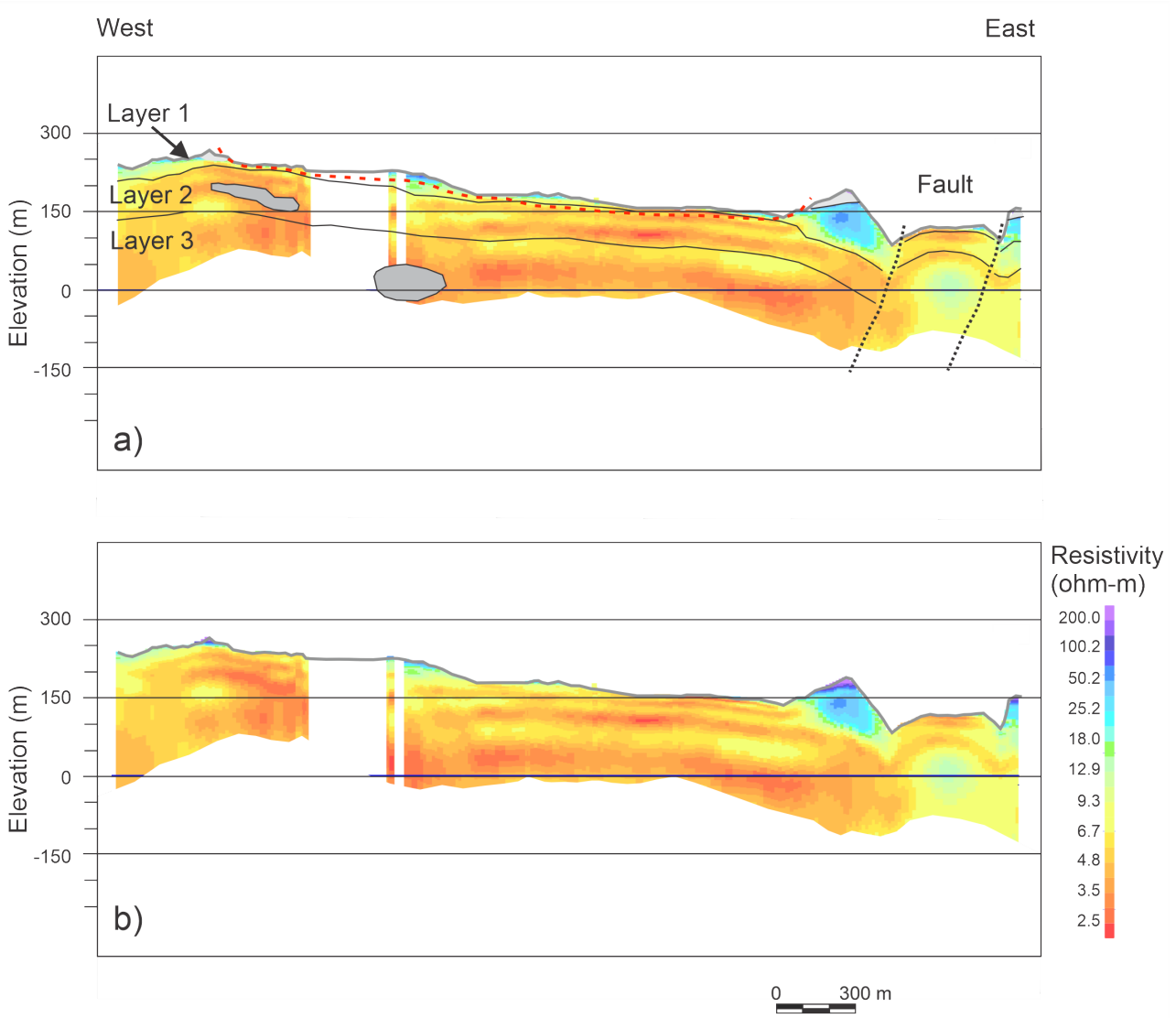

Figure A1.7 Te Puia Springs Line 600601 resistivity section. The section is plotted from south to north. The vertical exaggeration is 2:1. The data below the DOI are masked. (a) Interpreted section showing the primary layers 1–4, the zone of high resistivity at the surface (light shading) and the zones of low resistivity (medium shading). (b) Section without interpretation. The gaps in the profile are associated with buildings and roads that resulted in noisy data being removed from the processing.

A1.2 Mangahauini Survey

This appendix contains the interpreted and un-interpreted sections from each of the flight lines from Mangahauini Gorge.

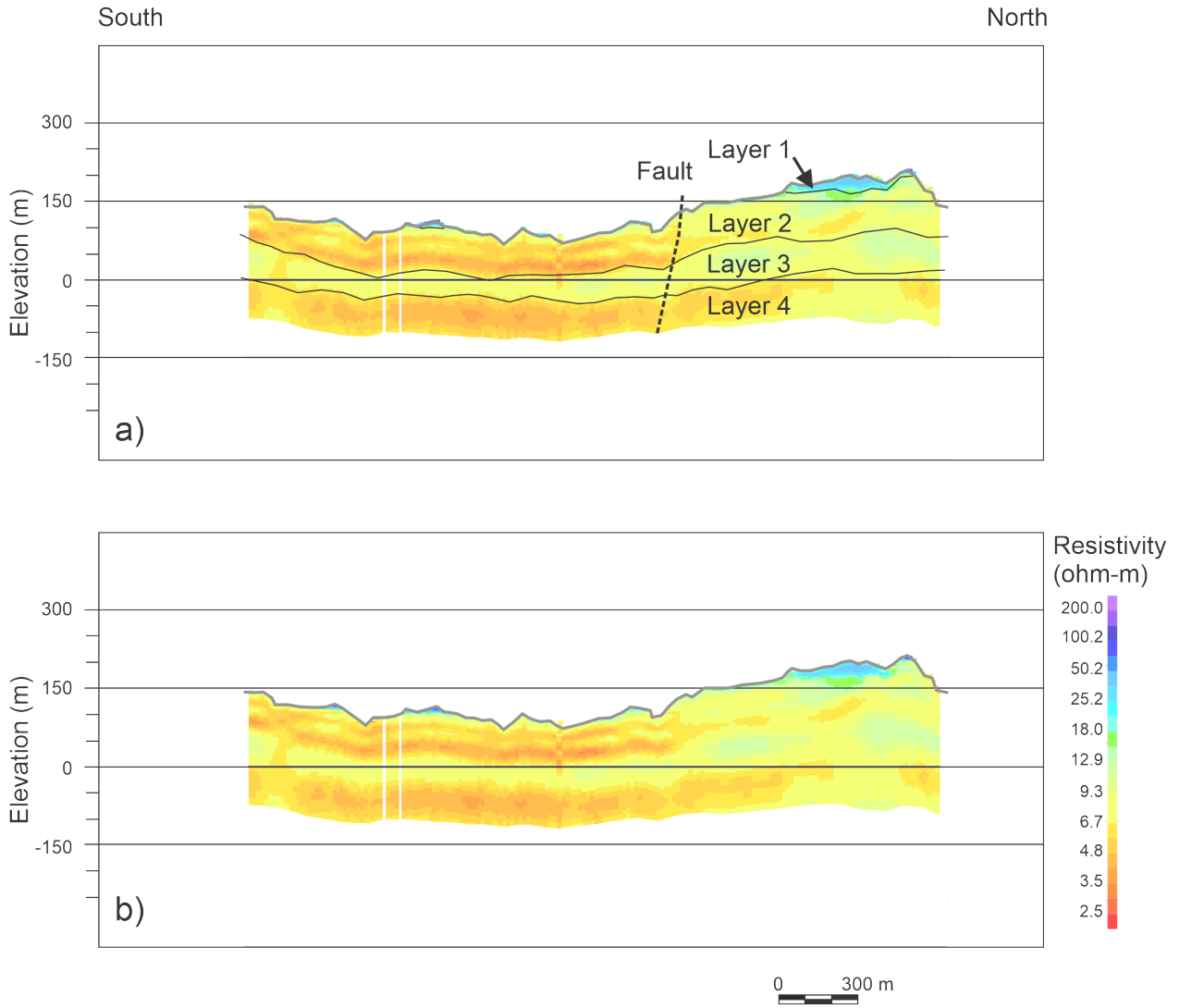

Figure A1.8 Mangahauini Line 700001 resistivity section. The section is plotted from south to north. The vertical exaggeration is 2:1. (a) Interpreted section showing the primary layers 1–4, the zone of high resistivity at the surface (light shading) and the zones of low resistivity (medium shading). (b) Section without interpretation. The gaps in the profile are associated with buildings and roads that resulted in noisy data being removed from the processing.

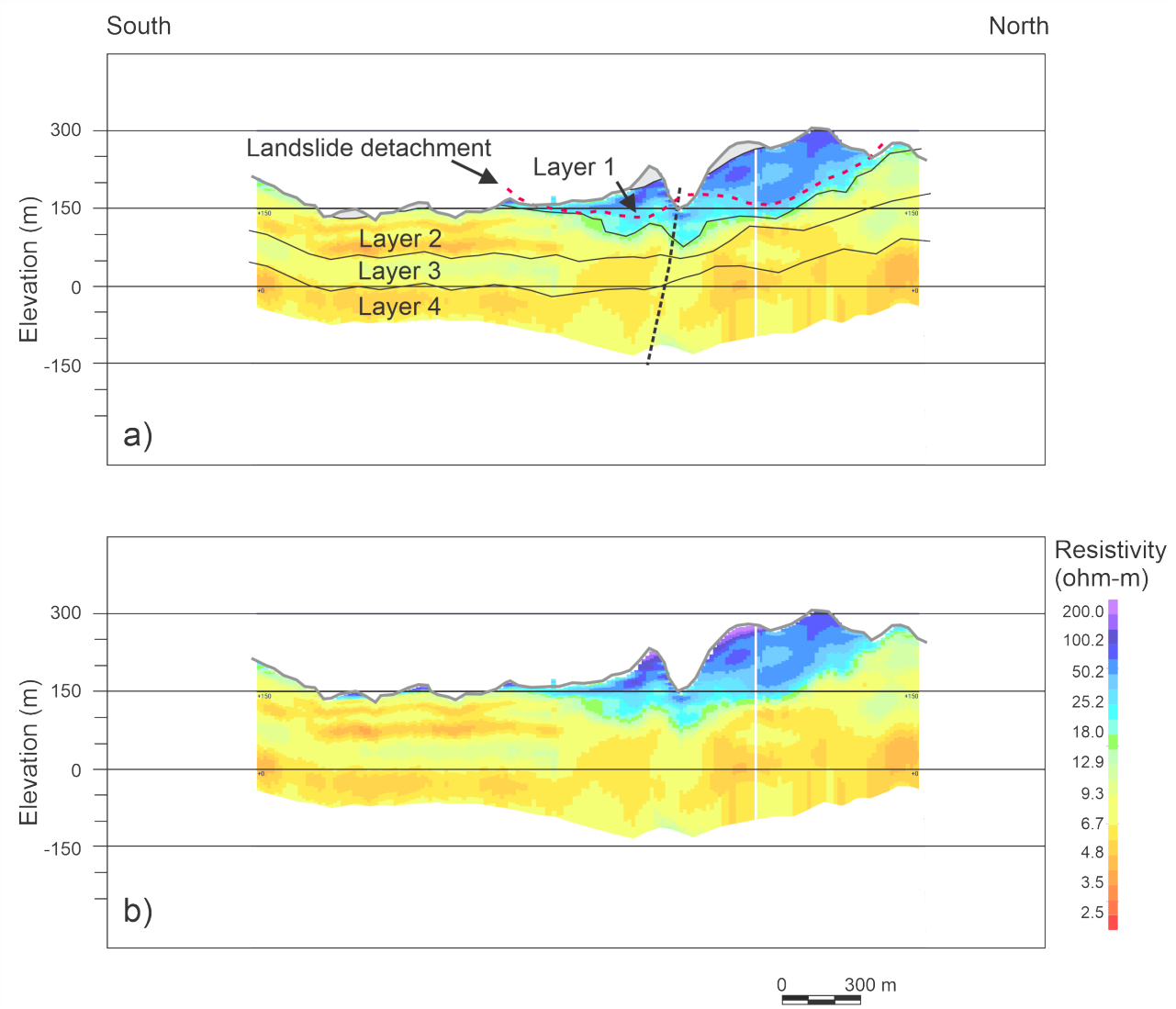

Figure A1.9 Mangahauini Line 700101 resistivity section. The section is plotted from south to north. The vertical exaggeration is 2:1. (a) Interpreted section showing the primary layers 1–4, the zone of high resistivity at the surface (light shading) and the zones of low resistivity (medium shading). (b) Section without interpretation. The gaps in the profile are associated with buildings and roads that resulted in noisy data being removed from the processing.

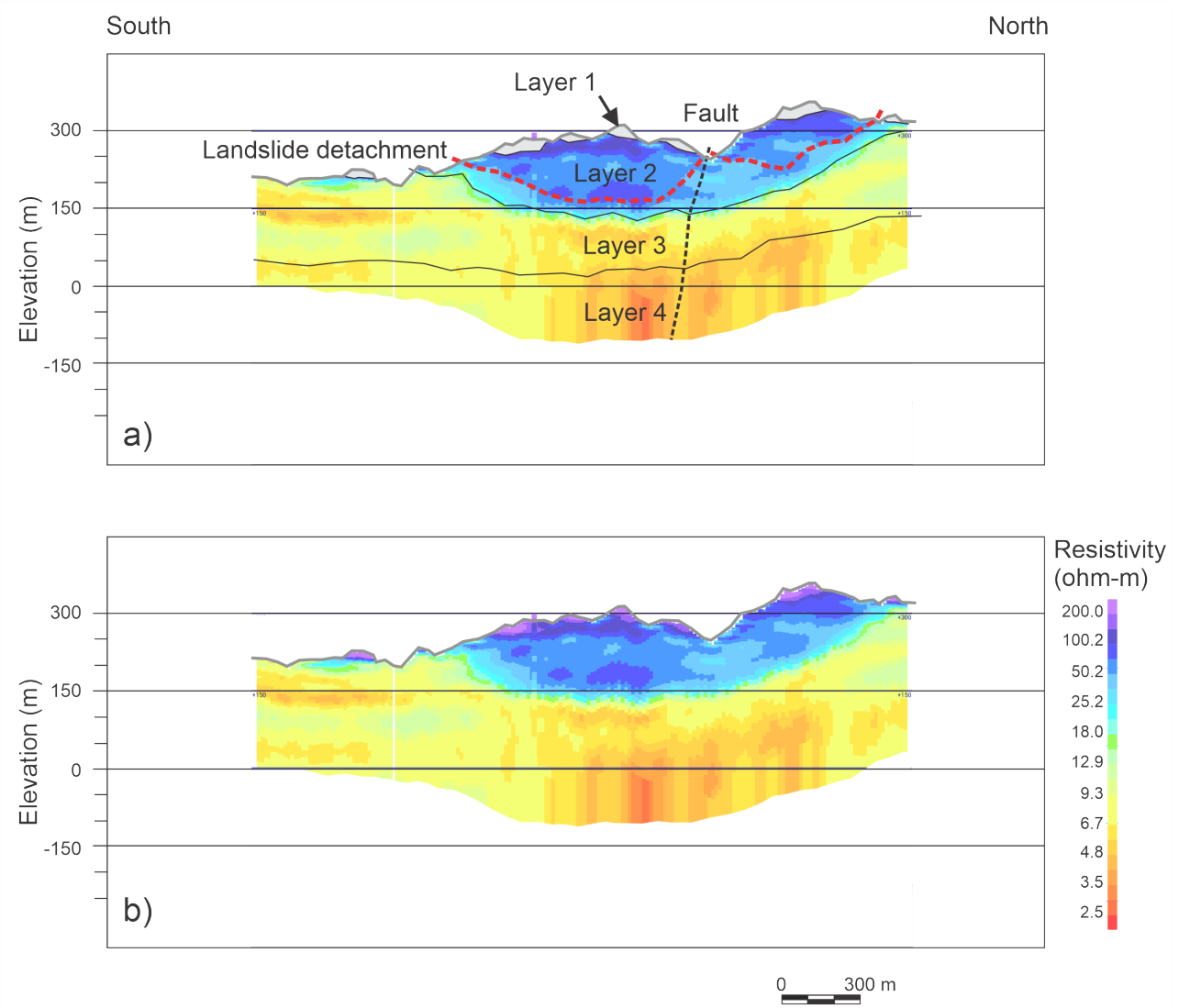

Figure A1.10 Mangahauini Line 700201 resistivity section. The section is plotted from south to north. The vertical exaggeration is 2:1. (a) Interpreted section showing the primary layers 1–4, the zone of high resistivity at the surface (light shading) and the zones of low resistivity (medium shading). (b) Section without interpretation. The gaps in the profile are associated with buildings and roads that resulted in noisy data being removed from the processing.

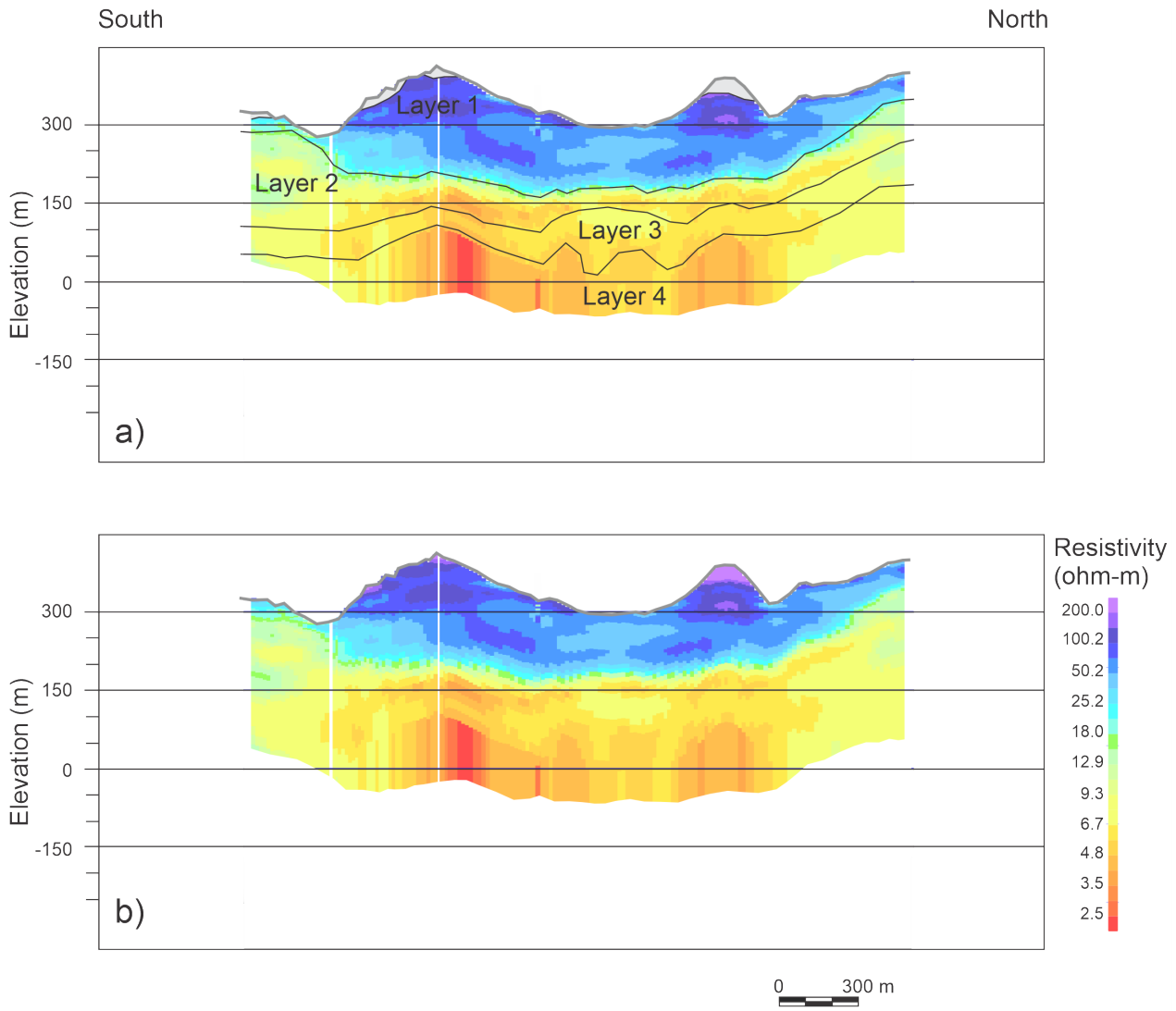

Figure A1.11 Mangahauini Line 703001 resistivity section. The section is plotted from south to north. The vertical exaggeration is 2:1. (a) Interpreted section showing the primary layers 1–4, the zone of high resistivity at the surface (light shading) and the zones of low resistivity (medium shading). (b) Section without interpretation. The gaps in the profile are associated with buildings and roads that resulted in noisy data being removed from the processing.

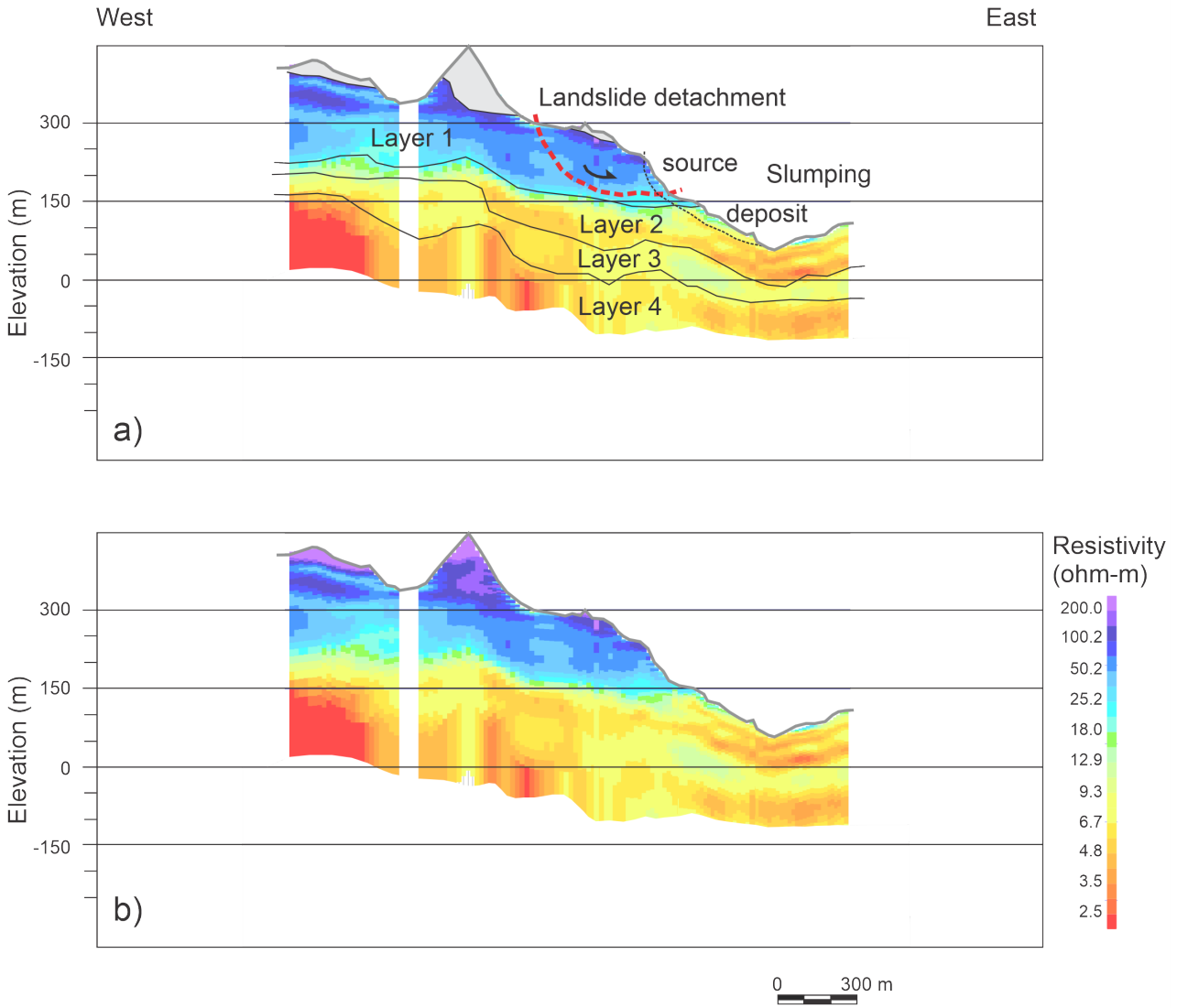

Figure A1.12 Mangahauini Line 700401 resistivity section. The section is plotted from west to east. The vertical exaggeration is 2:1. (a) Interpreted section showing the primary layers 1–4, the zone of high resistivity at the surface (light shading) and the zones of low resistivity (medium shading). (b) Section without interpretation. The gaps in the profile are associated with buildings and roads that resulted in noisy data being removed from the processing.

earthsciences.nz